Computers and Geotechnics 62 (2014) 136–153

Contents lists available at ScienceDirect

Computers and Geotechnics

journal homepage: www.elsevier.com/locate/compgeo

Analysis of laterally loaded pile groups in multilayered elastic soil

R. Salgado *, F.S. Tehrani, M. Prezzi

Purdue University, United States

A R T I C L E I N F O

Article history:
Received 28 December 2013
Received in revised form 6 June 2014
Accepted 8 July 2014
Available online 14 August 2014

Keywords:
Pile foundations
Laterally loaded piles
Pile groups
Elastic analyses

A B S T R A C T

The paper presents a semi-analytical method of calculating the response of a pile group. The approach is based on tying the displacement at any point of the soil mass around a pile or group of piles to the displacements experienced by the piles themselves. This is done by multiplying the pile displacements by decay functions. Application of the principle of minimum potential energy and calculus of variations to the resulting displacement field formulation leads to the differential equations for the soil and piles. Solution of these differential equations using finite differences and the method of eigenvectors leads to the desired displacement field in the soil and deflection profiles of the piles. The method produces displacement fields that are very close to those produced by the finite element method at a fraction of the cost. To illustrate the ease of application of the method, it is then used to prepare pile group efficiency charts for some typical soil modulus profiles.

1. Introduction

1.1. The problem of the laterally loaded pile group

It is common for a single pile to not have enough capacity to sustain a structural load (as from a column in a frame structure) on its own, so pile groups capped by a reinforced concrete pile cap are very common in foundation engineering solutions. The present paper proposes a new solution for the problem illustrated in Fig. 1, which addresses the lateral loading of a group of n_p piles connected at the top by a rigid cap and installed in a soil profile consisting of n_{total} layers. The main aim of any analysis of this problem is to relate the total displacement of the pile cap to the load applied on it. Also of interest are estimates of the displacements that develop in the surrounding soil and what the internal forces in the piles are.

Horizontal forces may be due to wind, waves, traffic or seismic loadings. These loads are, in the end, transferred to the piles supporting the structures. The horizontal forces get transmitted to the pile cap and then to the top of individual piles as concentrated forces and/or moments. One of the challenging aspects of pile design under lateral loads is to determine the fraction of the total loading that gets distributed to each pile. Given the range of structures subject to significant lateral loading, there has been considerable research on the problem of laterally-loaded piles, an indicator of the importance of the problem and an indicator also of the lack of a definitive, satisfactory solution to the problem. The literature on the topic is reviewed next.

1.2. Analysis and design approaches

1.2.1. Subgrade reaction method

Analysis of laterally loaded piles was initially based on the concept of representing soil by discrete springs using Winkler's beam on elastic foundation approach [1]. However, this approach was modified to account for plastic deformation of soil (which starts at very small strains) by incorporating non-linearity in the springs [2,3]. Further development of this concept led to the *p*–*y* method, which is widely used today.

In the *p*–*y* method, load–displacement (*p*–*y*) curves are associated with different depths along the pile, and the pile deflections are calculated iteratively using the so-called *p*–*y* curves [4–8]. For routine design, the *p*–*y* method is the method of choice, as finite element analyses are too costly, but it suffers from limitations [9–16].

1.2.2. Continuum approach

The continuum approach assumes the pile as embedded in an elastic continuum. Classical work (e.g., [17,18]) on the problem of the laterally loaded pile group has relied on analytical and numerical elastic techniques and principles, often including the principle of superposition, to solve it. The variational approach has been used to set up the boundary value problem for a pile loaded laterally in an elastic medium with some assumptions on the form of the displacement field; analytical or numerical solution of the

* Corresponding author.
E-mail addresses: rodrigo@ecn.purdue.edu (R. Salgado), ftehrani@ecn.purdue.edu (F.S. Tehrani), mprezzi@ecn.purdue.edu (M. Prezzi).

http://dx.doi.org/10.1016/j.compgeo.2014.07.005
0266-352X/

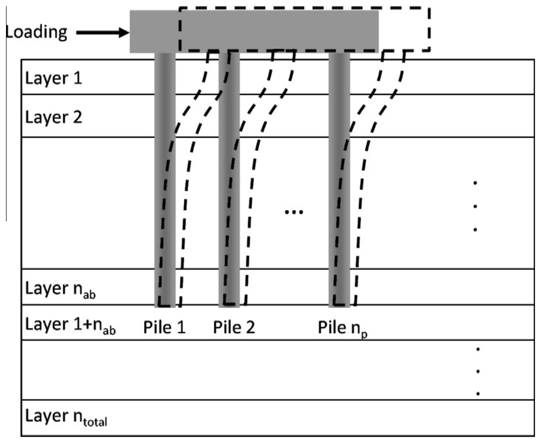

Fig. 1. A laterally loaded pile group in a multi-layered soil profile.

problem then led to the pile displacements for different boundary conditions [19,20]. Similarly, analyses of a laterally loaded pile installed in multi-layered soil were done by assuming mathematical forms for the displacement field in the soil and minimizing potential energy for the pile–soil system [21–23].

There has also been considerable work on use of numerical methods, particularly the finite element method [24–29] to study the laterally loaded pile group problem. The major advantage of numerical techniques is their flexibility in adapting to different geometries, boundary conditions and constitutive relationships. However, they are mostly problem-specific and computationally intensive, requiring, in addition, both sufficient experience on the part of the analyst and time to properly set up the analysis. In contrast, linear elastic methods cannot be applied in practice without a measure of judgment, but provide insights into pile load response and establish the conceptual basis for more realistic methods of analysis.

1.3. Pile group analysis and goals of the present paper

Field and model experiments have shown that pile group response to lateral loads is extremely complex and depends on many factors, including loading conditions, pile end restraints, pile arrangement and spacing, and the stiffness of each pile relative to the other piles and the soil [30–37]. In early research, displacement and load distribution among the piles were determined considering the effect of soil as elastic springs [38–40]. The most commonly used method of analysis today is the p–y multiplier technique. Based on full-scale tests of pile groups, it is known that, all other things being equal, a pile group deflects more than an isolated pile loaded to a load equal to the average load per pile in the group [25,41] because the soil stiffness is reduced due to the overlapping of deformation zones of neighboring piles. The p–y multiplier approach accounts for this by using multipliers (with value less than one) to reduce the ordinates of the single-pile p–y curve so that it can then be applied to each individual pile in the group. These multipliers have typically been back-calculated from experimental and numerical results [42–45,36,46,47]. The multiplier values are problem-specific, and there is no rational method available that can be used to predict the multipliers in a generalized way.

An evaluation of the different available methods [48] revealed that no single method was adequate in analyzing all aspects of pile groups, such as pile–soil–pile interaction, position and spacing of piles, and the relative stiffness of the piles. Deficiencies of the different methods have been reported by other researchers as well [49–51]. The existing methods for analyzing the laterally-loaded pile problem suffer from one or more of the following limitations: (1) need for important assumptions and approximations, (2) analyses that are difficult to use in practice or that do not provide much insight into the problem or (3) continued reliance on representation of the soil by springs. This paper presents an analysis of laterally-loaded pile groups in multi-layered, elastic soil media. The analysis is based on the assumption that the displacements at points in the soil is a function of the displacements of each pile in the group but the analysis does not rely on the superposition principle, which means there are no restrictions on its future use to a material that is not linear elastic. With the formulation of the displacement field established, the principle of minimum potential energy (or, more generally, the principle of virtual work) can be used to set up the formulation. The analysis is equally applicable to single piles (by simply making the number of piles equal to 1). The analysis has the strengths that it is based on proper physics; it is easy to use once it has been coded; and, being a continuum mechanics-based solution, it establishes the basis for future improvements, including use of more realistic constitutive models.

2. Theoretical framework

2.1. Displacement, strain and stress fields

The displacement $\{u(x,y,z)\}$ at any point in the soil mass around a pile group is linked to the displacement experienced by each pile in the group. The lateral component of $\{u(x,y,z)\}$ in the soil can then be expressed as the summation, for all n_p piles in the group, of the product of the lateral displacement $w_i(z)$ of pile i by a dissipation or decay function $f_i(x,y)$ associated with pile i. Each of these n_p decay functions varies between 1 at the location of the specific pile the decay function is associated with and zero both at the locations of all the other piles and at an infinite distance from the pile group (in practical terms, at the boundaries of the domain used to approximate the soil half space). One of the important advantages of this approach is that this assumption on soil displacement can be made regardless of the constitutive model used for the soil, i.e., it is not an application of the superposition principle, with the important implication that the approach is not restricted to an elastic model of the soil. The displacement field may be assumed more or less complex, making it more or less realistic.

In this paper, we assume a form for the displacement field in terms of Cartesian coordinates and assume a linear-elastic model for the soil. The simplest possible displacement function around a pile group is given by:

$$\begin{aligned} u_x &= \sum_{i=1}^{n_p} w_i(z) f_i(x,y) \\ u_y &= u_z = 0 \end{aligned} \tag{1}$$

where $f_i(x,y)$ is the decay function that attenuates the displacement $w_i(z)$ induced by the ith pile across the domain. Eq. (1) applies regardless of the shapes of the cross sections of the piles and, as we will show, produces excellent results despite its simplicity. Differentiation of (1) leads to the infinitesimal strain field (positive if contractive):

$$\varepsilon_{kl} = -\frac{1}{2}(u_{k,l} + u_{l,k}) \tag{2}$$

$$\begin{bmatrix} \varepsilon_{xx} \\ \varepsilon_{yy} \\ \varepsilon_{zz} \\ \varepsilon_{xy} \\ \varepsilon_{xz} \\ \varepsilon_{yz} \end{bmatrix} = \begin{bmatrix} -\frac{\partial u_x}{\partial x} \\ -\frac{\partial u_y}{\partial y} \\ -\frac{\partial u_z}{\partial z} \\ -\frac{1}{2}\left(\frac{\partial u_x}{\partial y} + \frac{\partial u_y}{\partial x}\right) \\ -\frac{1}{2}\left(\frac{\partial u_x}{\partial z} + \frac{\partial u_z}{\partial x}\right) \\ -\frac{1}{2}\left(\frac{\partial u_y}{\partial z} + \frac{\partial u_z}{\partial y}\right) \end{bmatrix} = \begin{bmatrix} -\sum_{i=1}^{n_p} w_i(z) \frac{\partial f_i(x,y)}{\partial x} \\ 0 \\ 0 \\ -\frac{1}{2}\left(\sum_{i=1}^{n_p} w_i(z) \frac{\partial f_i(x,y)}{\partial y}\right) \\ -\frac{1}{2}\left(\sum_{i=1}^{n_p} \frac{dw_i(z)}{dz} f_i(x,y)\right) \\ 0 \end{bmatrix} \tag{3}$$

The elastic stress–strain relations

$$\sigma_{kl} = 2\mu\varepsilon_{kl} + \lambda\varepsilon_{mm}\delta_{kl} \tag{4}$$

produce the elastic stresses:

$$\begin{bmatrix} \sigma_{xx} \\ \sigma_{yy} \\ \sigma_{zz} \\ \sigma_{xy} \\ \sigma_{xz} \\ \sigma_{yz} \end{bmatrix} = \begin{bmatrix} 2G_s+\lambda_s & \lambda_s & \lambda_s & 0 & 0 & 0 \\ \lambda_s & 2G_s+\lambda_s & \lambda_s & 0 & 0 & 0 \\ \lambda_s & \lambda_s & 2G_s+\lambda_s & 0 & 0 & 0 \\ 0 & 0 & 0 & 2G_s & 0 & 0 \\ 0 & 0 & 0 & 0 & 2G_s & 0 \\ 0 & 0 & 0 & 0 & 0 & 2G_s \end{bmatrix} \begin{bmatrix} \varepsilon_{xx} \\ \varepsilon_{yy} \\ \varepsilon_{zz} \\ \varepsilon_{xy} \\ \varepsilon_{xz} \\ \varepsilon_{yz} \end{bmatrix} \tag{5}$$

2.2. Potential energy and energy minimization

The strain energy density can be expressed as:

$$\frac{1}{2}\sigma_{kl}\varepsilon_{kl} = \frac{1}{2}\left(\sigma_{xx}\varepsilon_{xx} + 2\sigma_{xy}\varepsilon_{xy} + 2\sigma_{xz}\varepsilon_{xz}\right) \tag{6}$$

The total potential energy of the soil–pile system, including both internal and external potential energies, is given as:

$$\Pi = \frac{1}{2}\sum_{i=1}^{n_p} E_iI_i\int_{z=0}^{z=L_p}\left(\frac{d^2w_i(z)}{dz^2}\right)^2 dz + \frac{1}{2}\int_{\Omega_{soil}}\sigma_{kl}\varepsilon_{kl}d\Omega_{soil} - \sum_{i=1}^{n_p}F_iw_i(z)|_{z=0} + \sum_{i=1}^{n_p}M_i\frac{dw_i(z)}{dz}\bigg|_{z=0} \tag{7}$$

where E_iI_i is the flexural rigidity of pile i, and F_i and M_i are the external lateral load and moment acting at the head of pile i.

Application of the principle of minimum potential energy to the pile–soil system requires that we take the first variation of the potential energy and require that it be zero ($\delta\Pi = 0$). Taking the first variation of Π, as expressed in (7), we get:

$$\delta\Pi = \sum_{i=1}^{n_p}E_iI_i\int_{z=0}^{z=L_p}\delta\left(\frac{d^2w_i(z)}{dz^2}\right)\left(\frac{d^2w_i(z)}{dz^2}\right)dz + \frac{1}{2}\int_{\Omega_{soil}}\delta\left(\sigma_{xx}\varepsilon_{xx} + 2\sigma_{xy}\varepsilon_{xy} + 2\sigma_{xz}\varepsilon_{xz}\right)d\Omega_{soil} - \sum_{i=1}^{n_p}F_i\delta w_i(z)|_{z=0} + \sum_{i=1}^{n_p}M_i\delta\left(\frac{dw_i(z)}{dz}\right)_{z=0} = 0 \tag{8}$$

which, fully expanded after stress and strain substitutions and with recognition that the elastic properties may vary with depth z, becomes:

$$\begin{aligned}\delta\Pi = &\sum_{i=1}^{n_p}E_iI_i\int_{z=0}^{z=L_p}\delta\left(\frac{d^2w_i(z)}{dz^2}\right)\left(\frac{d^2w_i(z)}{dz^2}\right)dz \\ &+\sum_{i=1}^{n_p}\sum_{j=1}^{n_p}\left\{\iiint_{\Omega_{soil}}(2G_s(z)+\lambda_s(z))\left[\delta w_i(z)w_j(z)\frac{\partial f_i(x,y)}{\partial x}\frac{\partial f_j(x,y)}{\partial x}\right]dxdydz\right. \\ &+\iiint_{\Omega_{soil}}(2G_s(z)+\lambda_s(z))\left[w_i(z)w_j(z)\delta\left(\frac{\partial f_i(x,y)}{\partial x}\right)\frac{\partial f_j(x,y)}{\partial x}\right]dxdydz \\ &+\iiint_{\Omega_{soil}}G_s(z)\left[\delta w_i(z)w_j(z)\frac{\partial f_i(x,y)}{\partial y}\frac{\partial f_j(x,y)}{\partial y}\right]dxdydz \\ &+\iiint_{\Omega_{soil}}G_s(z)\left[w_i(z)w_j(z)\delta\left(\frac{\partial f_i(x,y)}{\partial y}\right)\frac{\partial f_j(x,y)}{\partial y}\right]dxdydz \\ &+\iiint_{\Omega_{soil}}G_s(z)\left[\delta\left(\frac{dw_i(z)}{dz}\right)\frac{dw_j(z)}{dz}f_i(x,y)f_j(x,y)\right]dxdydz \\ &\left.+\iiint_{\Omega_{soil}}G_s(z)\left[\frac{dw_i(z)}{dz}\frac{dw_j(z)}{dz}\delta f_i(x,y)f_j(x,y)\right]dxdydz\right\} \\ &-\sum_{i=1}^{n_p}F_i\delta w_i(z)|_{z=0}+\sum_{i=1}^{n_p}M_i\delta\left(\frac{dw_i(z)}{dz}\right)_{z=0}=0\end{aligned} \tag{9}$$

Each of the terms in (9) has a first variation of some variable. The next step is to collect terms containing common first variations and organize them into terms associated with the piles and terms associated with the soil domain. We start with terms containing variations of $w_i\,(z)$ and its derivatives:

$$\begin{aligned}&E_iI_i\int_{z=0}^{z=L_p}\delta\left(\frac{d^2w_i(z)}{dz^2}\right)\left(\frac{d^2w_i(z)}{dz^2}\right)dz \\ &+\sum_{j=1}^{n_p}\left\{\iiint_{\Omega_{soil}}(2G_s(z)+\lambda_s(z))\left[\delta w_i(z)w_j(z)\frac{\partial f_i(x,y)}{\partial x}\frac{\partial f_j(x,y)}{\partial x}\right]dxdydz\right. \\ &+\iiint_{\Omega_{soil}}G_s(z)\left[\delta w_i(z)w_j(z)\frac{\partial f_i(x,y)}{\partial y}\frac{\partial f_j(x,y)}{\partial y}\right]dxdydz \\ &\left.+\iiint_{\Omega_{soil}}G_s(z)\left[\delta\left(\frac{dw_i(z)}{dz}\right)\frac{dw_j(z)}{dz}f_i(x,y)f_j(x,y)\right]dxdydz\right\} \\ &-F_i\delta w_i(z)|_{z=0}+M_i\delta\left(\frac{dw_i(z)}{dz}\right)_{z=0}=0\end{aligned} \tag{10}$$

For a layered soil deposit, Eq. (10) becomes:

$$\begin{aligned}&E_iI_i\sum_{k=1}^{n_{ab}}\int_{H_{k-1}}^{H_k}\delta\left(\frac{d^2w_{i,k}(z)}{dz^2}\right)\left(\frac{d^2w_{i,k}(z)}{dz^2}\right)dz \\ &+\sum_{j=1}^{n_p}\left\{\sum_{k=1}^{n_{total}}\iiint_{\Omega_{layer\ k}}(2G_{s,k}(z)+\lambda_{s,k}(z))\left[\delta w_{i,k}(z)w_{j,k}(z)\frac{\partial f_i(x,y)}{\partial x}\frac{\partial f_j(x,y)}{\partial x}\right]dxdydz\right. \\ &+\sum_{k=1}^{n_{total}}\iiint_{\Omega_{layer\ k}}G_{s,k}(z)\left[\delta w_{i,k}(z)w_{j,k}(z)\frac{\partial f_i(x,y)}{\partial y}\frac{\partial f_j(x,y)}{\partial y}\right]dxdydz \\ &\left.+\sum_{k=1}^{n_{total}}\iiint_{\Omega_{layer\ k}}G_{s,k}(z)\left[\delta\left(\frac{dw_{i,k}(z)}{dz}\right)\frac{dw_{j,k}(z)}{dz}f_i(x,y)f_j(x,y)\right]dxdydz\right\} \\ &-F_i\delta w_{i,1}(z)|_{z=0}+M_i\delta\left(\frac{dw_{i,1}(z)}{dz}\right)_{z=0}=0\end{aligned} \tag{11}$$

where the sums are over layers, n_{ab} is the number of sub-layers above the pile base, and n_{total} is the total number of layers and sub layers.

Integration by parts and further simplification of (11) lead to:

$$\begin{aligned}&E_iI_i\sum_{k=1}^{n_{ab}}\left\{\left[\delta\left(\frac{dw_{i,k}(z)}{dz}\right)\left(\frac{d^2w_{i,k}(z)}{dz^2}\right)\right]_{H_{k-1}}^{H_k}-\left[\delta w_{i,k}\left(\frac{d^3w_{i,k}(z)}{dz^3}\right)\right]_{H_{k-1}}^{H_k}\right. \\ &\left.+\int_{H_{k-1}}^{H_k}\frac{d^4w_{i,k}(z)}{dz^4}\delta w_{i,k}dz\right\} \\ &+\sum_{j=1}^{n_p}\left\{\sum_{k=1}^{n_{total}}\int_{H_{k-1}}^{H_k}\left(k_{ij}^{z,k}(z)w_{j,k}(z)-t_{ij}^{z,k}(z)\frac{d^2w_{j,k}(z)}{dz^2}-\frac{dt_{ij}^{z,k}(z)}{dz}\frac{dw_{j,k}(z)}{dz}\right)\right. \\ &\left.\delta w_{i,k}(z)dz+\sum_{k=1}^{n_{total}}\left[\delta w_{i,k}\left(t_{ij}^{z,k}(z)\frac{dw_{j,k}(z)}{dz}\right)\right]_{H_{k-1}}^{H_k}\right\}-F_i\delta w_{i,1}(z)|_{z=0} \\ &+M_i\delta\left(\frac{dw_{i,1}(z)}{dz}\right)_{z=0}=0\end{aligned} \tag{12}$$

where

$$k_{ij}^{z,k} = \iint_{xy}\left[(2G_{s,k}(z)+\lambda_{s,k}(z))\frac{\partial f_i(x,y)}{\partial x}\frac{\partial f_j(x,y)}{\partial x} + G_{s,k}(z)\frac{\partial f_i(x,y)}{\partial y}\frac{\partial f_j(x,y)}{\partial y}\right.$$

$$t_{ij}^{z,k} = \iint_{xy}G_{s,k}(z)f_i(x,y)f_j(x,y)dxdy$$

are integrals evaluated only over the soil domain for each layer k.

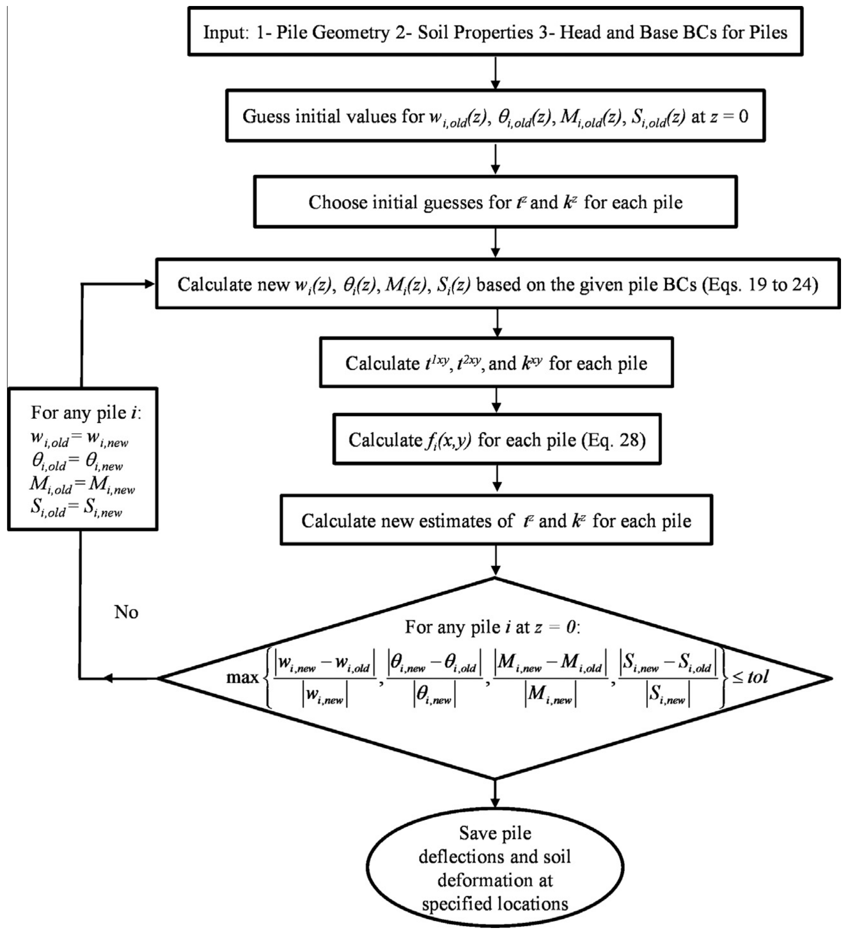

Fig. 2. Algorithm for solving the problem of laterally loaded pile groups.

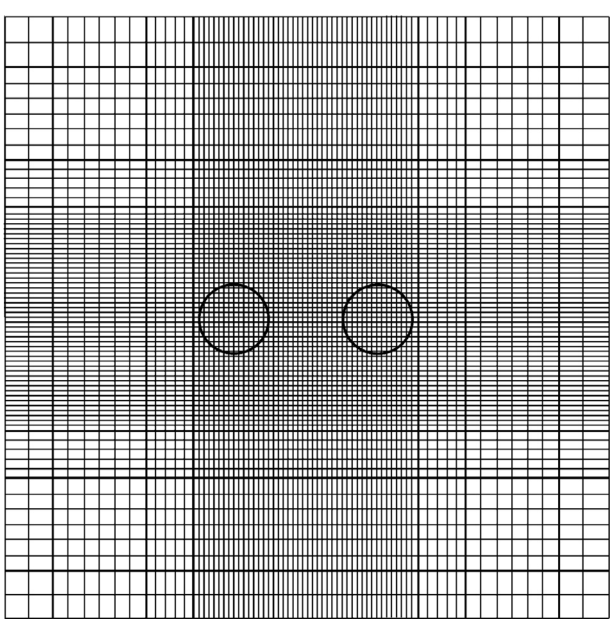

Fig. 3. Schematic grid for a pile group-soil domain on x–y plane.

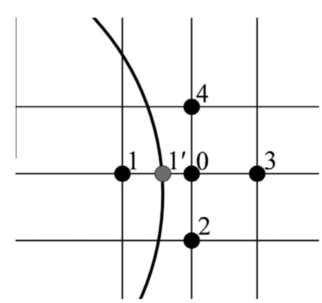

Fig. 4. Five-point stencil near the pile domain.

Collecting the terms containing $\delta f_i(x,y)$ in Eq. (9) follows:

$$\sum_{j=1}^{n_p}\left\{\iiint_{\Omega_{soil}}(2G_s(z)+\lambda_s(z))\left[w_i(z)w_j(z)\delta\left(\frac{\partial f_i(x,y)}{\partial x}\right)\frac{\partial f_j(x,y)}{\partial x}\right]dxdydz\right.$$
$$+\iiint_{\Omega_{soil}}G_s(z)\left[w_i(z)w_j(z)\delta\left(\frac{\partial f_i(x,y)}{\partial y}\right)\frac{\partial f_j(x,y)}{\partial y}\right]dxdydz$$
$$\left.+\iiint_{\Omega_{soil}}G_s(z)\left[\frac{dw_i(z)}{dz}\frac{dw_j(z)}{dz}\delta f_i(x,y)f_j(x,y)\right]dxdydz\right\}=0 \quad (13)$$

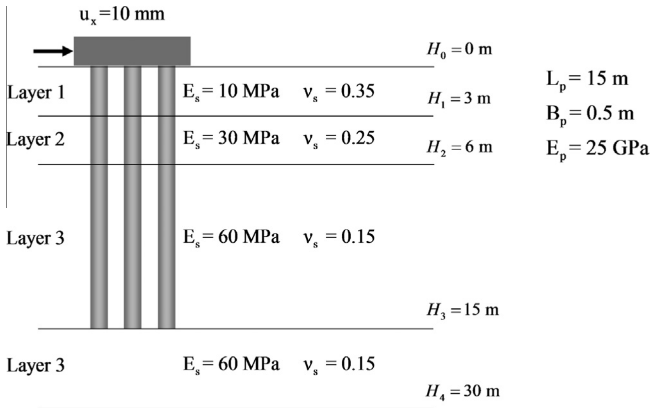

Fig. 5. Soil profile used in validation of the method of analysis.

Rewriting of Eq. (13) produces:

$$\sum_{j=1}^{n_p}\left\{t_{ij}^{1xy}\left[\int_{-\infty}^{+\infty}\delta f_i(x,y)\frac{\partial f_j(x,y)}{\partial x}dy\right]_{x\to-\infty}^{x\to+\infty}-t_{ij}^{1xy}\iint_{\Omega_{soil}}\frac{\partial^2 f_j(x,y)}{\partial x^2}\delta f_i(x,y)dxdy\right.$$
$$+t_{ij}^{2xy}\left[\int_{-\infty}^{+\infty}\delta f_i(x,y)\frac{\partial f_j(x,y)}{\partial y}dx\right]_{y\to-\infty}^{y\to+\infty}-t_{ij}^{2xy}\iint_{\Omega_{soil}}\frac{\partial^2 f_j(x,y)}{\partial y^2}\delta f_i(x,y)dxdy$$
$$\left.+k_{ij}^{xy}\iint_{\Omega_{soil}}f_j(x,y)\delta f_i(x,y)dxdy\right\}=0 \tag{14}$$

where

$$t_{ij}^{1xy}=\int_{z=0}^{\infty}(2G_s(z)+\lambda_s(z))w_i(z)w_j(z)dz=\sum_{k=1}^{n_{total}}\int_{H_{k-1}}^{H_k}(2G_{s,k}(z)+\lambda_{s,k}(z))w_{i,k}(z)w_{j,k}(z)dz$$
$$t_{ij}^{2xy}=\int_{z=0}^{\infty}G_s(z)w_i(z)w_j(z)dz=\sum_{k=1}^{n_{total}}\int_{H_{k-1}}^{H_k}G_{s,k}(z)w_{i,k}(z)w_{j,k}(z)dz$$
$$k_{ij}^{xy}=\int_{z=0}^{\infty}G_s(z)\frac{dw_i(z)}{dz}\frac{dw_j(z)}{dz}dz=\sum_{k=1}^{n_{total}}\int_{H_{k-1}}^{H_k}G_{s,k}(z)\frac{dw_{i,k}(z)}{dz}\frac{dw_{j,k}(z)}{dz}dz$$

2.3. Differential equations

Eq. (9) is valid only if each of the coefficients of the first variations appearing in it is zero. This requirement leads to the differential equations and boundary conditions for the laterally loaded pile group problem. These differential equations are known as Euler–Lagrange differential equations, and they produce the functions $w_i(z)$ and $f_i(x,y)$ that minimize the potential energy of the system. Using Eq. (12), the Euler–Lagrange equation for the ith pile and kth layer is given as:

$$E_iI_i\frac{d^4w_{i,k}(z)}{dz^4}+\sum_{j=1}^{n_p}\left\{-t_{ij}^{z,k}(z)\frac{d^2w_{j,k}(z)}{dz^2}-\frac{dt_{ij}^{z,k}(z)}{dz}\frac{dw_{j,k}(z)}{dz}+k_{ij}^{z,k}(z)w_{j,k}(z)\right\}=0 \tag{15}$$

for $z \leqslant L_p$, and

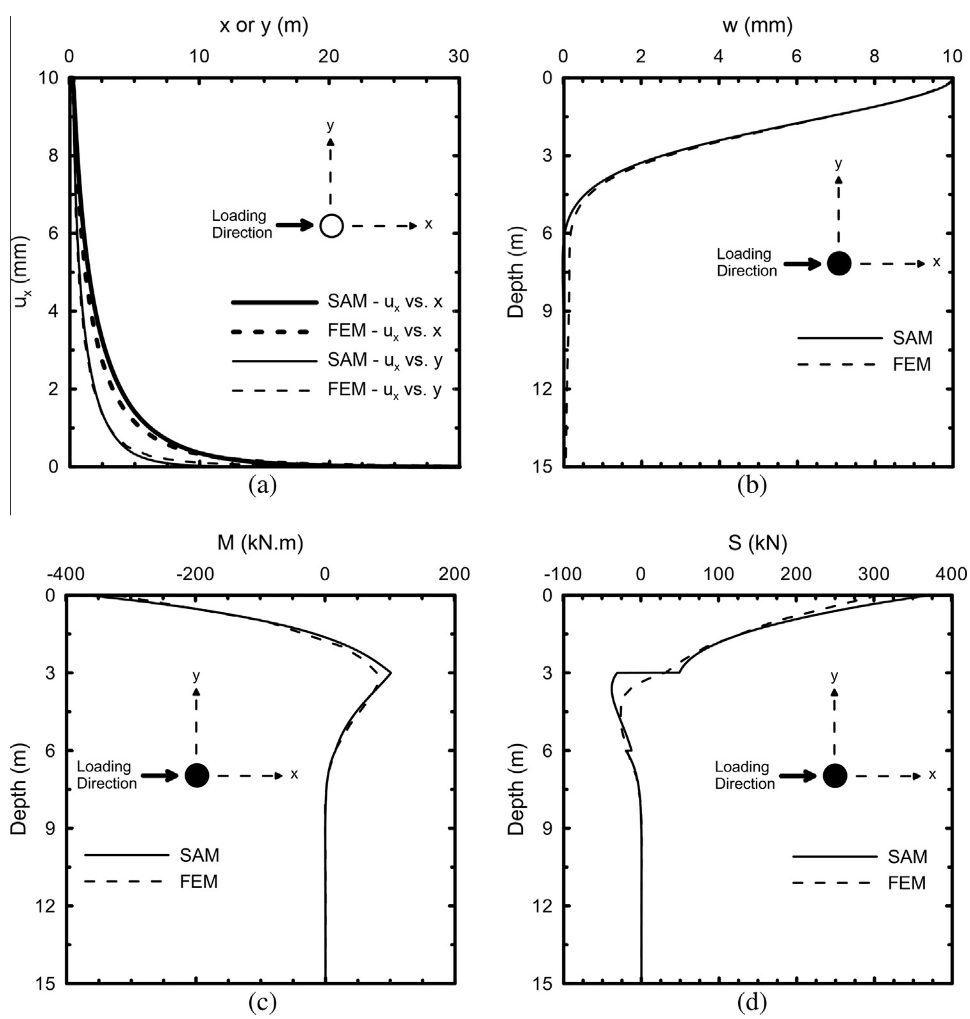

Fig. 6. Soil and pile deflection properties due to 10 mm pile head deflection of a single pile: (a) lateral displacement at ground elevation, (b) lateral displacement of the pile in the direction of the applied load, (c) bending moment, and (d) shear force.

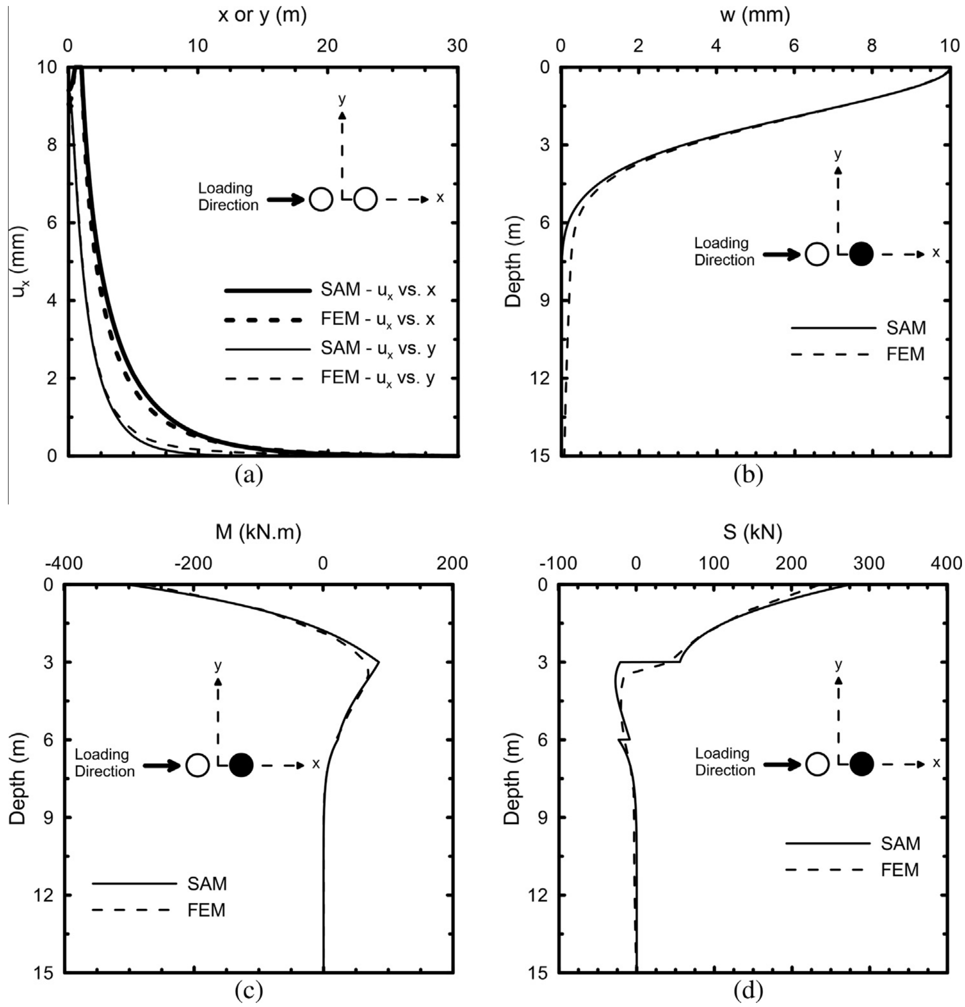

Fig. 7. Soil and pile deflection properties due to 10 mm pile head deflection of a 1 × 2 pile group: (a) lateral displacement at ground elevation, (b) lateral displacement of the pile in the direction of the applied load (c) bending moment and (d) shear force.

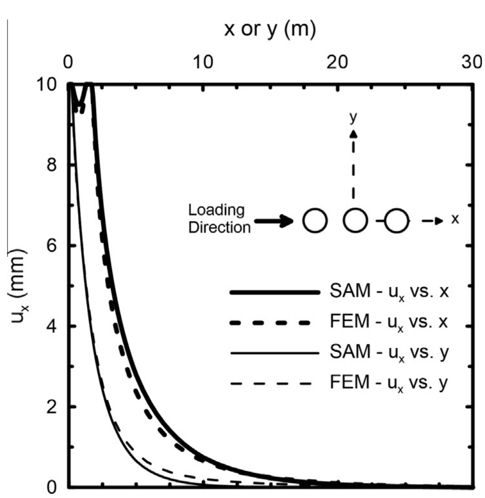

Fig. 8. Lateral displacement at ground elevation for the 1 × 3 pile group.

$$\sum_{j=1}^{n_p}\left\{-t_{ij}^{z,k}(z)\frac{d^2w_{j,k}(z)}{dz^2}-\frac{dt_{ij}^{z,k}(z)}{dz}\frac{dw_{j,k}(z)}{dz}+k_{ij}^{z,k}(z)w_{j,k}(z)\right\}=0 \qquad (16)$$

for $z > L_p$.

Eqs. (15) and (16) are differential equations with variable coefficients. For linear elastic soil, the coefficients $t_{ij}^{z,k}$ and $k_{ij}^{z,k}$ for every layer do not vary with depth, which suggests Eqs. (15) and (16) can be rewritten as:

$$E_iI_i\frac{d^4w_{i,k}(z)}{dz^4}+\sum_{j=1}^{n_p}\left\{-t_{ij}^{z,k}\frac{d^2w_{j,k}(z)}{dz^2}+k_{ij}^{z,k}w_{j,k}(z)\right\}=0 \qquad (17)$$

for $z \leqslant L_p$, and

$$\sum_{j=1}^{n_p}\left\{-t_{ij}^{z,k}\frac{d^2w_{j,k}(z)}{dz^2}+k_{ij}^{z,k}w_{j,k}(z)\right\}=0 \qquad (18)$$

for $z > L_p$, which are ordinary differential equations with constant coefficients.

The boundary conditions for the ith pile also follow from Eq. (12). At $z = 0$:

$$\begin{cases} w_{i,1}(z)=w_{i0} \\ \text{or} \\ E_iI_i\frac{d^3w_{i,1}(z)}{dz^3}-\sum_{j=1}^{n_p}t_{ij}^{z,1}\frac{dw_{j,1}(z)}{dz}=F_i \end{cases} \qquad (19)$$

and

$$\begin{cases} \left.\frac{dw_{i,1}(z)}{dz}\right|_{z=0}=\theta_{i0} \\ \text{or} \\ E_iI_i\frac{d^2w_{i,1}(z)}{dz^2}=M_i \end{cases} \qquad (20)$$

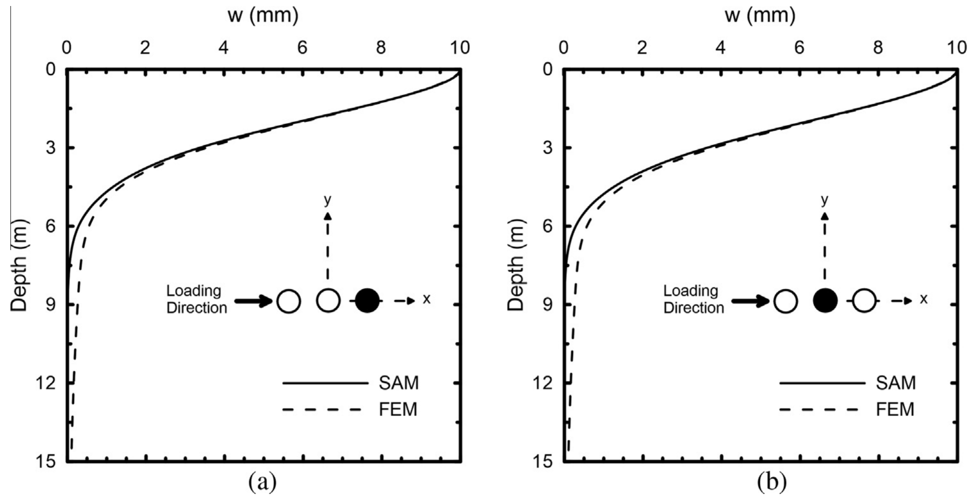

Fig. 9. Deflection of the (a) corner pile and (b) center pile in the 1 × 3 pile group.

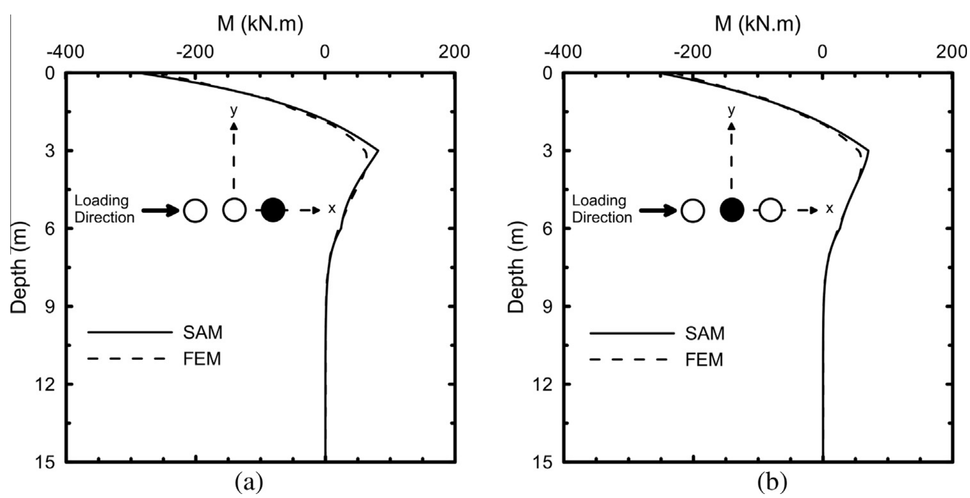

Fig. 10. Bending moment along the (a) corner pile and (b) center pile in the 1 × 3 pile group.

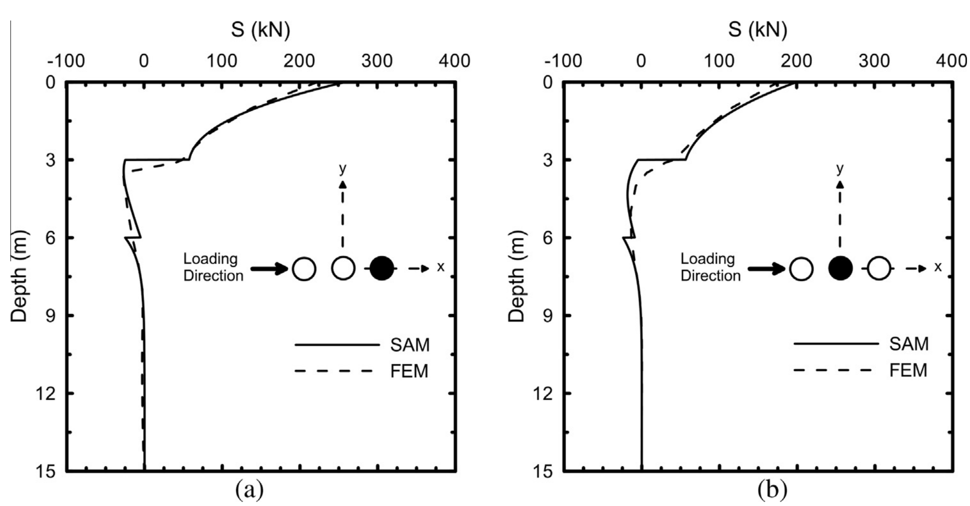

Fig. 11. Shear force along the (a) corner pile and (b) center pile in the 1 × 3 pile group.

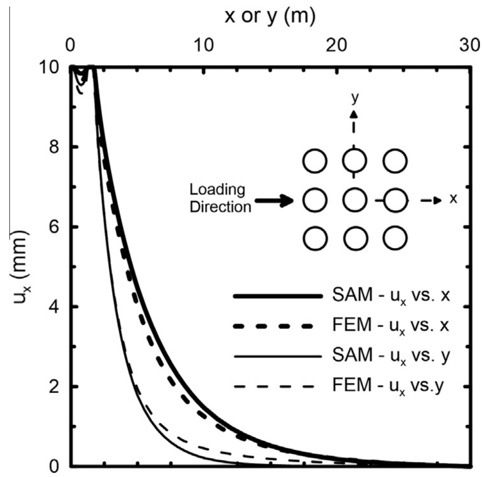

Fig. 12. Lateral displacement at ground elevation for the 3 × 3 pile group.

At $z = H_k < L_p$:

$$\begin{cases} w_{i,k} = w_{i,k+1} \\ E_iI_i \frac{d^3w_{i,k}(z)}{dz^3} - \sum_{j=1}^{n_p} t_{ij}^{z,k} \frac{dw_{j,k}(z)}{dz} = E_iI_i \frac{d^3w_{i,k+1}(z)}{dz^3} - \sum_{j=1}^{n_p} t_{ij}^{z,k+1} \frac{dw_{j,k+1}(z)}{dz} \\ \frac{dw_{i,k}(z)}{dz} = \frac{dw_{i,k+1}(z)}{dz} \\ E_iI_i \frac{d^2w_{i,k}(z)}{dz^2} = E_iI_i \frac{d^2w_{i,k+1}(z)}{dz^2} \end{cases} \tag{21}$$

At $z = H_k = L_p$:

$$\begin{cases} w_{i,k} = w_{i,k+1} \\ E_iI_i \frac{d^3w_{i,k}(z)}{dz^3} - \sum_{j=1}^{n_p} t_{ij}^{z,k} \frac{dw_{j,k}(z)}{dz} = -\sum_{j=1}^{n_p} t_{ij}^{z,k+1} \frac{dw_{j,k+1}(z)}{dz} \\ E_iI_i \frac{d^2w_{i,k}(z)}{dz^2} = 0 \end{cases} \tag{22}$$

for a free pile base, and

$$\begin{cases} w_{i,k} = 0 \\ w_{i,k+1} = 0 \\ \left.\frac{dw_{i,k}(z)}{dz}\right|_{z=L_p} = 0 \end{cases} \tag{23}$$

for a fixed pile base.

At $z = H_k > L_p$ and $k < n_{total}$:

$$\begin{cases} w_{i,k} = w_{i,k+1} \\ \sum_{j=1}^{n_p} t_{ij}^{z,k} \frac{dw_{j,k}(z)}{dz} = \sum_{j=1}^{n_p} t_{ij}^{z,k+1} \frac{dw_{j,k+1}(z)}{dz} \end{cases} \tag{24}$$

Finally, at infinite depth, $z = H_{n_{total}} \to \infty$ and $w_{i,k} = 0$.

From Eq. (14), the Euler–Lagrange equation for the decay function associated with pile i is given as:

$$\sum_{j=1}^{n_p} \left\{ -t_{ij}^{1xy} \frac{\partial^2 f_j(x,y)}{\partial x^2} - t_{ij}^{2xy} \frac{\partial^2 f_j(x,y)}{\partial y^2} + k_{ij}^{xy} f_j(x,y) \right\} = 0 \tag{25}$$

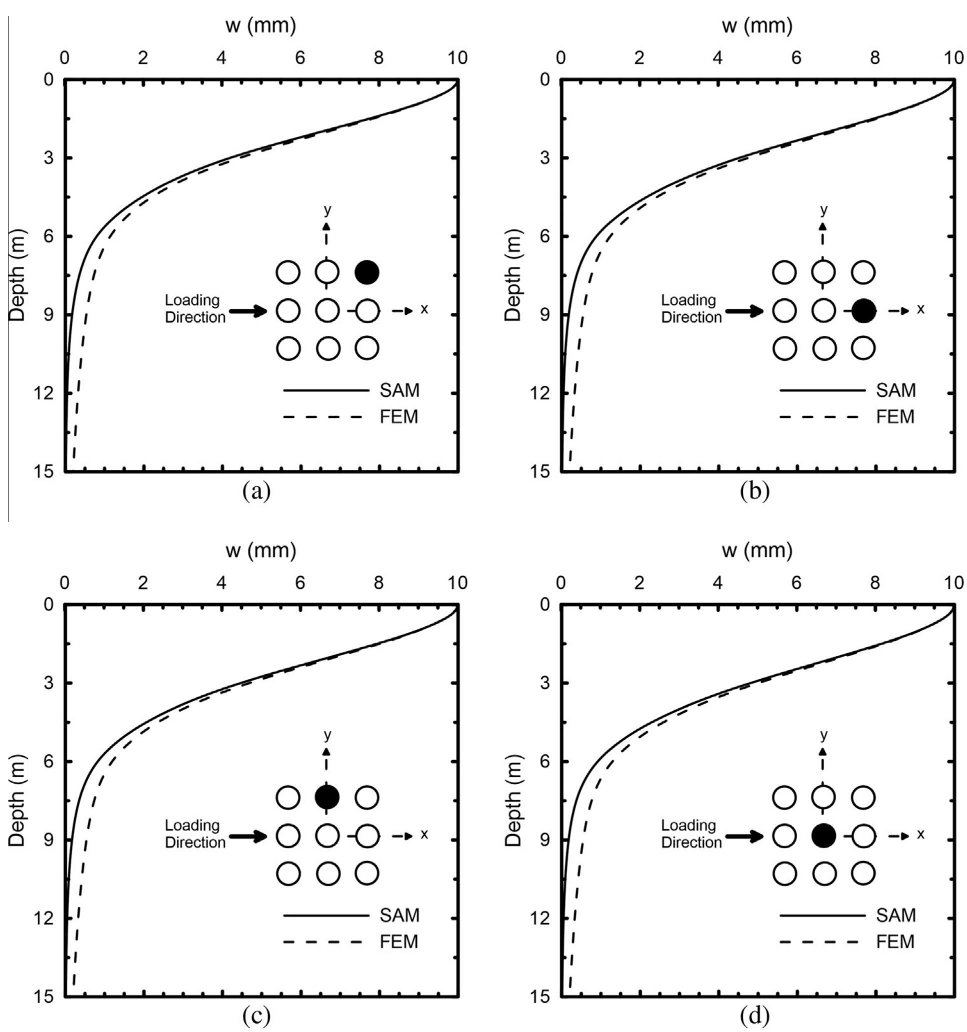

Fig. 13. Deflection of the (a) corner pile, (b) edge pile on the x axis, (c) edge pile on the y axis and (d) center pile in the 3 × 3 pile group.

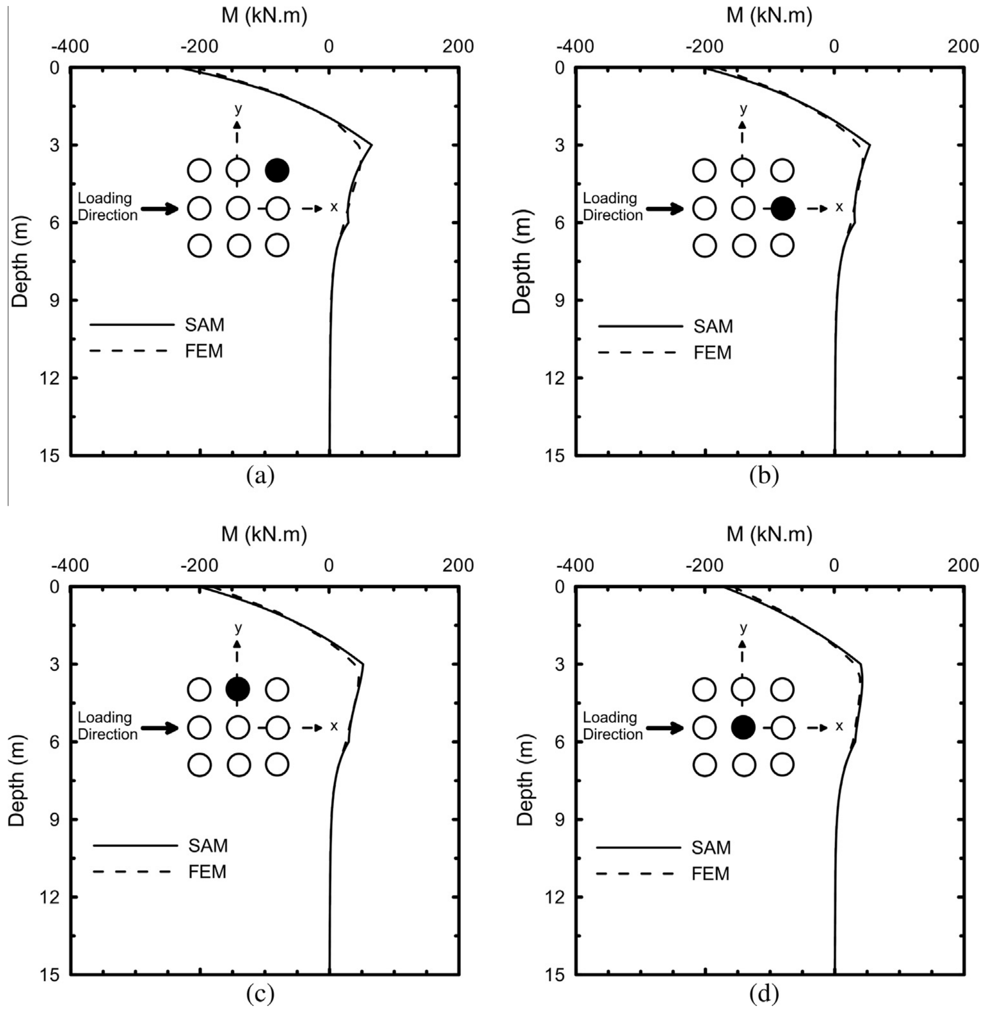

Fig. 14. Bending moment along the (a) corner pile, (b) edge pile on the x axis, (c) edge pile on the y axis and (d) center pile in the 3 × 3 pile group.

with boundary conditions:

$$f_i(x,y) = \begin{cases} 1 & \text{at pile } i \\ 0 & \text{at other piles} \end{cases} \tag{26}$$

This means that the value of the decay function associated with the ith pile is 1 within the cross section of pile i and zero within the cross section of all the other piles. Additionally, at infinity ($x \to \pm\infty$ or $y \to \pm\infty$), it also tends to zero.

Eq. (25) is a system of coupled partial differential equations that needs to be solved numerically along with the analytical solutions of Eqs. (17) and (18) to derive the responses of the pile and the displacement field in the soil. Rewriting of Eq. (25) as:

$$-t_{ii}^{1xy}\frac{\partial^2 f_i(x,y)}{\partial x^2} - t_{ii}^{2xy}\frac{\partial^2 f_i(x,y)}{\partial y^2} + k_{ii}^{xy} f_i(x,y) + \sum_{j=1, j\neq i}^{n_p}\left\{-t_{ij}^{1xy}\frac{\partial^2 f_j(x,y)}{\partial x^2} - t_{ij}^{2xy}\frac{\partial^2 f_j(x,y)}{\partial y^2} + k_{ij}^{xy} f_j(x,y)\right\} = 0 \tag{27}$$

allows us to more clearly separate the physical effects that the analysis represents. The fourth term of the left side of Eq. (27) includes the effect of the other piles in the group on the contribution of pile i to the displacement field (as represented by f_i) in the soil domain. This coupling was found to be superfluous in terms of accuracy because the most important coupling between the piles in the group is captured by Eqs. (17) and (18). Additionally, because the values of the coefficients of Eq. (25) are within a narrow range for all piles, consideration of that term can produce an ill-conditioned coefficient matrix for large groups. A simplifying assumption that eliminates this shortcoming and reduces computation time is to simply neglect the fourth term of the left side of Eq. (27), which leaves us with the following equation to describe the effect of any pile in the group on the surrounding soil:

$$-t_{ii}^{1xy}\frac{\partial^2 f_i(x,y)}{\partial x^2} - t_{ii}^{2xy}\frac{\partial^2 f_i(x,y)}{\partial y^2} + k_{ii}^{xy} f_i(x,y) = 0 \tag{28}$$

2.4. Semi-analytical solution for pile deflection profiles

We use the eigenvalue method for solving the coupled ordinary differential equations for the pile deflections. Eq. (17) are a system of 4th-order ODEs for layers above the pile base, and Eq. (18) are a system of second-order ODEs for layers below the pile base. For a layer k above the pile base, the eigenvalue method for solving a system of 4th-order ODEs is based on expressing the differential equations as a matrix equation:

$$[A]\{\omega_k\} = \{\omega_k'\} \tag{29}$$

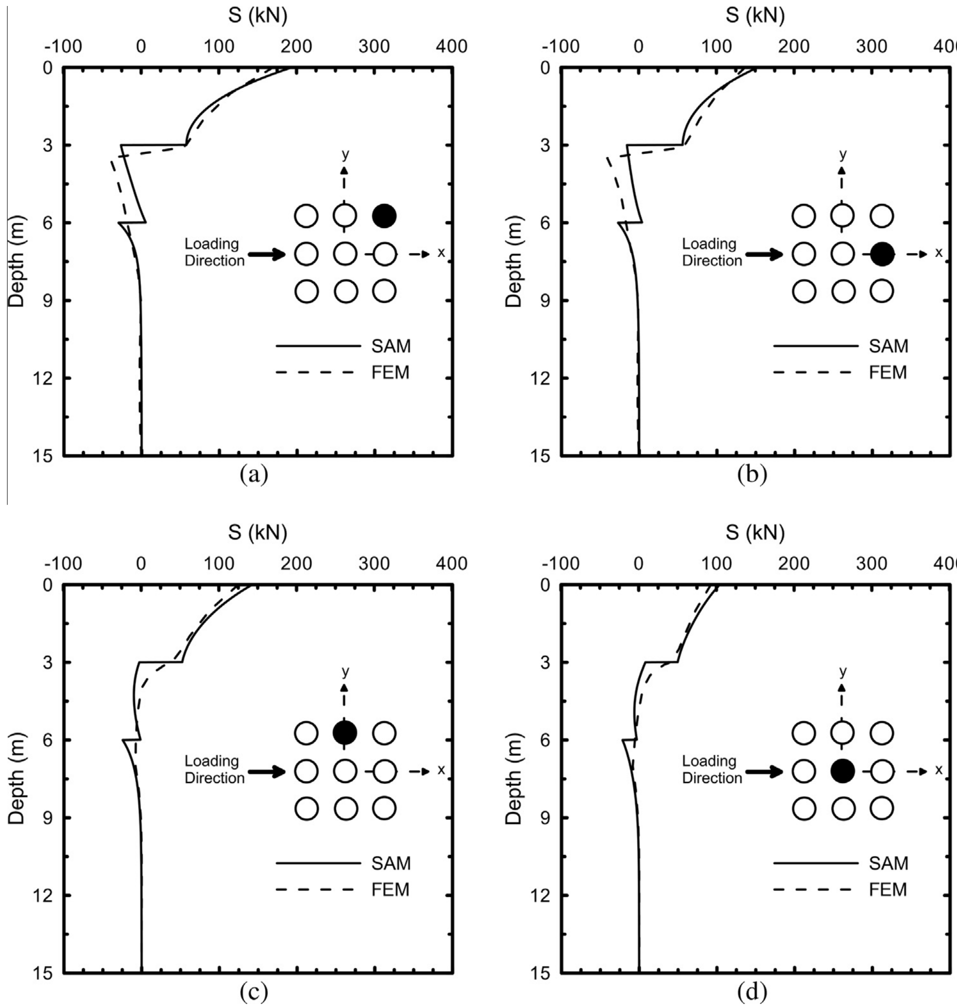

Fig. 15. Shear force along the (a) corner pile, (b) edge pile on the x axis, (c) edge pile on the y axis and (d) center pile in the 3×3 pile group.

Table 1
Computational effort for each pile group analysis.

Case	FEM		SAM		
	Number of elements	Total CPU time (s)	Number of surface nodes	Number of iterations	Total CPU time (s)
Single pile	353,266	1357.2	15,376	5	27.8
1 × 2 Pile group	541,490	2493.4	24,676	7	71.1
1 × 3 Pile group	512,760	1909.5	23,188	6	134.5
3 × 3 Pile group	503,766	1511.5	24,649	6	350.8

where

$$\{\omega_k\} = \Big\{w_{1,k}(z), w'_{1,k}(z), w''_{1,k}(z), w'''_{1,k}(z), \ldots, w_{n_p,k}(z), w'_{n_p,k}(z), w''_{n_p,k}(z), w'''_{n_p,k}(z)\Big\}^T \tag{30}$$

$$\{\omega'_k\} = \Big\{w'_{1,k}(z), w''_{1,k}(z), w'''_{1,k}(z), w^{(4)}_{1,k}(z), \ldots, w'_{n_p,k}(z), w''_{n_p,k}(z), w''_{n_p,k}(z), w^{(4)}_{n_p,k}(z)\Big\}^T \tag{31}$$

and the coefficient matrix $[A]$ has the following block form:

$$[A] = \begin{bmatrix} [A_{11}] & \cdots & [A_{1j}] & \cdots & [A_{1n_p}] \\ \vdots & \ddots & \vdots & \ddots & \vdots \\ [A_{i1}] & \cdots & [A_{ij}] & \cdots & [A_{in_p}] \\ \vdots & \ddots & \vdots & \ddots & \vdots \\ [A_{n_p1}] & \cdots & [A_{n_pj}] & \cdots & [A_{n_pn_p}] \end{bmatrix} \tag{32}$$

where

$$[A_{ij}] = \begin{bmatrix} 0 & \delta_{ij} & 0 & 0 \\ 0 & 0 & \delta_{ij} & 0 \\ 0 & 0 & 0 & \delta_{ij} \\ -k^{z,k}_{ij}/E_iI_i & 0 & t^{z,k}_{ij}/E_iI_i & 0 \end{bmatrix} \tag{33}$$

in which δ_{ij} is the Kronecker delta that is equal to unity when i and j are equal, otherwise zero.

Solution of the ODE system represented by (29) is given by:

$$\{\omega_k\} = \sum_{i=1}^{4n_p} c_i \exp(\lambda_i z)\{v_i\} \tag{34}$$

where c_i are arbitrary integration constants that are determined by applying the boundary conditions at the interfaces of layer k, λ_i are the eigenvalues of the coefficient matrix $[A]$, and $\{v_i\}$ is the ith eigenvector of the coefficient matrix $[A]$.

For any pile j in the group, the deflection and its derivatives within the kth layer are given by:

$$w_{j,k} = \sum_{i=1}^{4n_p} c_i \exp(\lambda_i z) v_{(4j-3),i} \tag{35}$$

$$\frac{dw_{j,k}}{dz} = \sum_{i=1}^{4n_p} c_i \exp(\lambda_i z) v_{(4j-2),i} \tag{36}$$

$$\frac{d^2 w_{j,k}}{dz^2} = \sum_{i=1}^{4n_p} c_i \exp(\lambda_i z) v_{(4j-1),i} \tag{37}$$

$$\frac{d^3 w_{j,k}}{dz^3} = \sum_{i=1}^{4n_p} c_i \exp(\lambda_i z) v_{4j,i} \tag{38}$$

where as an example, $v_{(4j-3),i}$ is the $(4j-3)$th component of the ith eigenvector.

Below the pile base, we can rewrite Eq. (18) for the kth layer as:

$$-[T]\{w''\} + [K]\{w\} = 0 \tag{39}$$

where

$$\{w\} = \{w_{1,k}(z), \ldots, w_{n_p,k}(z)\}^T \tag{40}$$

$$\{w''\} = \left\{w''_{1,k}(z), \ldots, w''_{n_p,k}(z)\right\}^T \tag{41}$$

$$[T] = \begin{bmatrix} t_{11}^{z,k} & \cdots & t_{1j}^{z,k} & \cdots & t_{1n_p}^{z,k} \\ \vdots & \ddots & \vdots & \ddots & \vdots \\ t_{i1}^{z,k} & \cdots & t_{ij}^{z,k} & \cdots & t_{in_p}^{z,k} \\ \vdots & \ddots & \vdots & \ddots & \vdots \\ t_{n_p1}^{z,k} & \cdots & t_{n_pj}^{z,k} & \cdots & t_{n_pn_p}^{z,k} \end{bmatrix} \tag{42}$$

and

$$[K] = \begin{bmatrix} k_{11}^{z,k} & \cdots & k_{1j}^{z,k} & \cdots & k_{1n_p}^{z,k} \\ \vdots & \ddots & \vdots & \ddots & \vdots \\ k_{i1}^{z,k} & \cdots & k_{ij}^{z,k} & \cdots & k_{in_p}^{z,k} \\ \vdots & \ddots & \vdots & \ddots & \vdots \\ k_{n_p1}^{z,k} & \cdots & k_{n_pj}^{z,k} & \cdots & k_{n_pn_p}^{z,k} \end{bmatrix} \tag{43}$$

To produce an equation similar to Eq. (29), we can write:

$$[T]\{w''\} = [K]\{w\} \tag{44}$$

or

$$\{w''\} = [T]^{-1}[K]\{w\} = [\Psi]\{w\} \tag{45}$$

Now we have the following relationship:

$$[B]\{\xi\} = \{\xi'\} \tag{46}$$

where

$$\{\xi\} = \left\{w_{1,k}(z), w'_{1,k}(z), \ldots, w_{n_p,k}(z), w'_{n_p,k}(z)\right\}^T \tag{47}$$

$$\{\xi'\} = \left\{w'_{1,k}(z), w''_{1,k}(z), \ldots, w'_{n_p,k}(z), w''_{n_p,k}(z)\right\}^T \tag{48}$$

$$[B] = \begin{bmatrix} [B_{11}] & \cdots & [B_{1j}] & \cdots & [B_{1n_p}] \\ \vdots & \ddots & \vdots & \ddots & \vdots \\ [B_{i1}] & \cdots & [B_{ij}] & \cdots & [B_{in_p}] \\ \vdots & \ddots & \vdots & \ddots & \vdots \\ [B_{n_p1}] & \cdots & [B_{n_pj}] & \cdots & [B_{n_pn_p}] \end{bmatrix} \tag{49}$$

$$[B_{ij}] = \begin{bmatrix} 0 & \delta_{ij} \\ \Psi_{ij} & 0 \end{bmatrix} \tag{50}$$

Solution of the ODE system represented by Eq. (46) is given by:

$$\{\xi_k\} = \sum_{i=1}^{2n_p} c_i \exp(\lambda_i z)\{v_i\} \tag{51}$$

where c_i are integration constants, λ_i are the eigenvalues of coefficient matrix $[B]$, and $\{v_i\}$ is the ith eigenvector of the coefficient matrix $[B]$.

For any pile j in the group, the deflection and its derivatives within the kth layer below the level of the pile base are given by:

$$w_{j,k} = \sum_{i=1}^{2n_p} c_i \exp(\lambda_i z) v_{(2j-1),i} \tag{52}$$

$$\frac{dw_{j,k}}{dz} = \sum_{i=1}^{2n_p} c_i \exp(\lambda_i z) v_{2j,i} \tag{53}$$

The solution vectors $\{\omega_k\}$ and $\{\xi_k\}$ may be complex vectors. We consider only the real part of these vectors to obtain the displacement along the pile.

2.5. Numerical determination of the decay functions $f_i(x,y)$

We use a 2D central-difference finite difference formulation to solve the decay function differential equations. In order to reduce computation time, we use unequal spacing to discretize the domain. As discussed in more detail in Appendix A, a five-point stencil was used to derive the discretized forms of the partial derivatives of $f_i(x,y)$.

The discretized form of the governing differential equations for the decay functions associated with pile i is:

$$\begin{aligned} &-t_{ii}^{1xy}\frac{\partial^2 f_i(x,y)}{\partial x^2} - t_{ii}^{2xy}\frac{\partial^2 f_i(x,y)}{\partial y^2} + k_{ii}^{xy} f_i(x,y) = \\ &-4t_{ii}^{1xy}\left[\frac{\Delta x_R f_i^{k-1,l} - (\Delta x_L + \Delta x_R) f_i^{k,l} + \Delta x_L f_i^{k+1,l}}{(\Delta x_L + \Delta x_R)(\Delta x_L^2 + \Delta x_R^2)}\right] \\ &-4t_{ii}^{2xy}\left[\frac{\Delta y_T f_i^{k,l-1} - (\Delta y_B + \Delta y_T) f_i^{k,l} + \Delta y_B f_i^{k,l+1}}{(\Delta y_B + \Delta y_T)(\Delta y_B^2 + \Delta y_T^2)}\right] + k_{ii}^{xy} f_i^{k,l} \Bigg\} = 0 \end{aligned} \tag{54}$$

Reordering and simplification of (54) produces:

$$\begin{aligned} &\left\{4t_{ii}^{1xy}\left(\frac{1}{\Delta x_L^2 + \Delta x_R^2}\right) + 4t_{ii}^{2xy}\left(\frac{1}{\Delta y_B^2 + \Delta y_T^2}\right) + k_{ii}^{xy}\right\} f_i^{k,l} \\ &- \frac{4t_{ii}^{1xy}}{(\Delta x_L + \Delta x_R)(\Delta x_L^2 + \Delta x_R^2)}\left(\Delta x_R f_i^{k-1,l} + \Delta x_L f_i^{k+1,l}\right) \\ &- \frac{4t_{ii}^{2xy}}{(\Delta y_B + \Delta y_T)(\Delta y_B^2 + \Delta y_T^2)}\left(\Delta y_T f_i^{k,l-1} + \Delta y_B f_i^{k,l+1}\right) = 0 \end{aligned} \tag{55}$$

2.6. Algorithm

With the formulation of the boundary-value problem complete, we turn to the algorithm to perform the calculations, which is shown in Fig. 2. The algorithm is based on feedback between the piles and the soil. The soil stiffness results from the pattern of deformation in the soil determined by the decay functions $f_i(x,y)$ and the pile displacements $w_i(z)$, which result in the quantities t^z and k^z that appear in the coefficients of the pile differential equations. Once the new pile displacement profiles are obtained by solution of the system of the pile differential equations, the quantities t^{1xy}, t^{2xy} and k^{xy}, which appear in the differential equations for the decay functions, can be calculated, allowing new estimates of the decay functions to be calculated and the cycle to restart. This process continues until convergence is achieved.

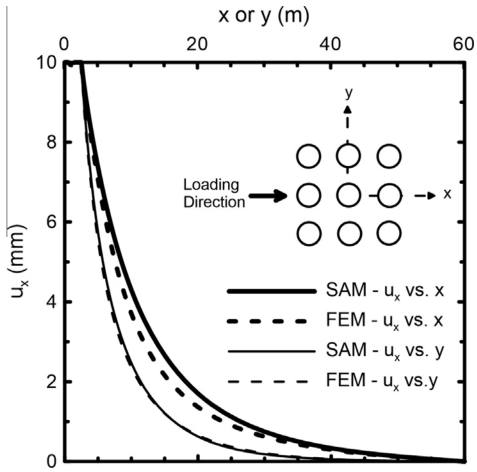

Fig. 16. Lateral displacement at ground elevation for the 3 × 3 pile group.

The solution starts by assuming initial values for the coefficients t^z and k^z for each layer; the pile deflections and their derivatives are then solved for using Eqs. (17) and (18). Once the pile deflection profiles are obtained, the coefficients t^{1xy}, t^{2xy}, and k^{xy} of the decay function differential equations are calculated; this is followed by calculation of the decay functions (Eq. (28)) and their partial derivatives. In the subsequent iteration, the values of the decay functions and their partial derivatives obtained in the previous step are used to recalculate the values of the coefficients t^z and k^z for each layer and the pile deflections in the current step. These steps are repeated until convergence, which is checked by comparing the current values of deflection, rotation, shear force, and bending moment of each pile at the pile head with values at the previous step and by enforcing a relative error less than the tolerance *tol*, for which a value of 10^{-3} was found to be sufficient. This check also ensured convergence of these quantities at other locations along the pile length.

3. Analysis validation

3.1. Grid size analysis

Solving the partial differential equations (PDEs) for the decay functions requires discretizing the domain in the *x*–*y* plane and solving the discretized form of the PDEs using the finite difference method. It is necessary to discretize the domain with sufficient accuracy using a fine grid to capture the shape of the pile and surrounding soil with sufficient accuracy, but it is equally important to do so while keeping computational costs down to reasonable levels. This was achieved by decomposing the domain into

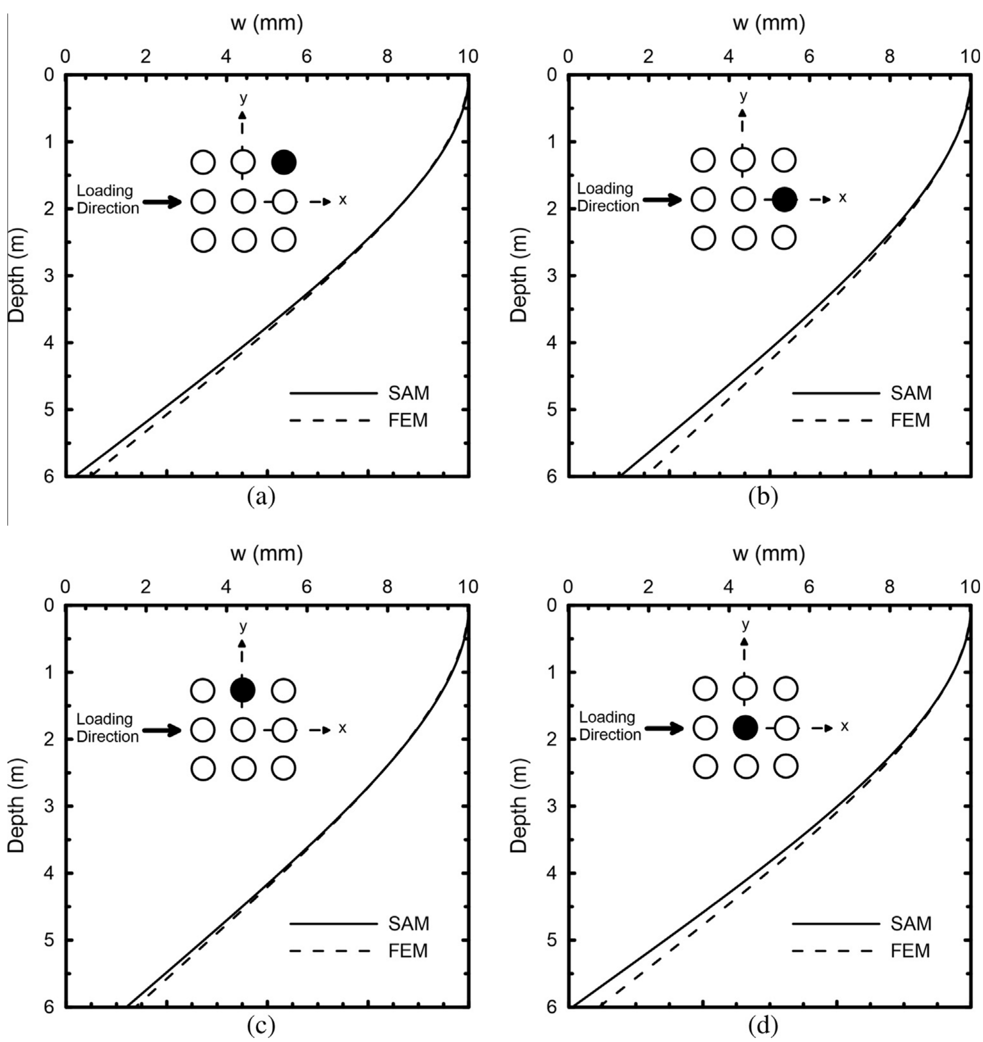

Fig. 17. Deflection of the (a) corner pile, (b) edge pile on the *x* axis, (c) edge pile on the *y* axis and (d) center pile in the 3 × 3 pile group.

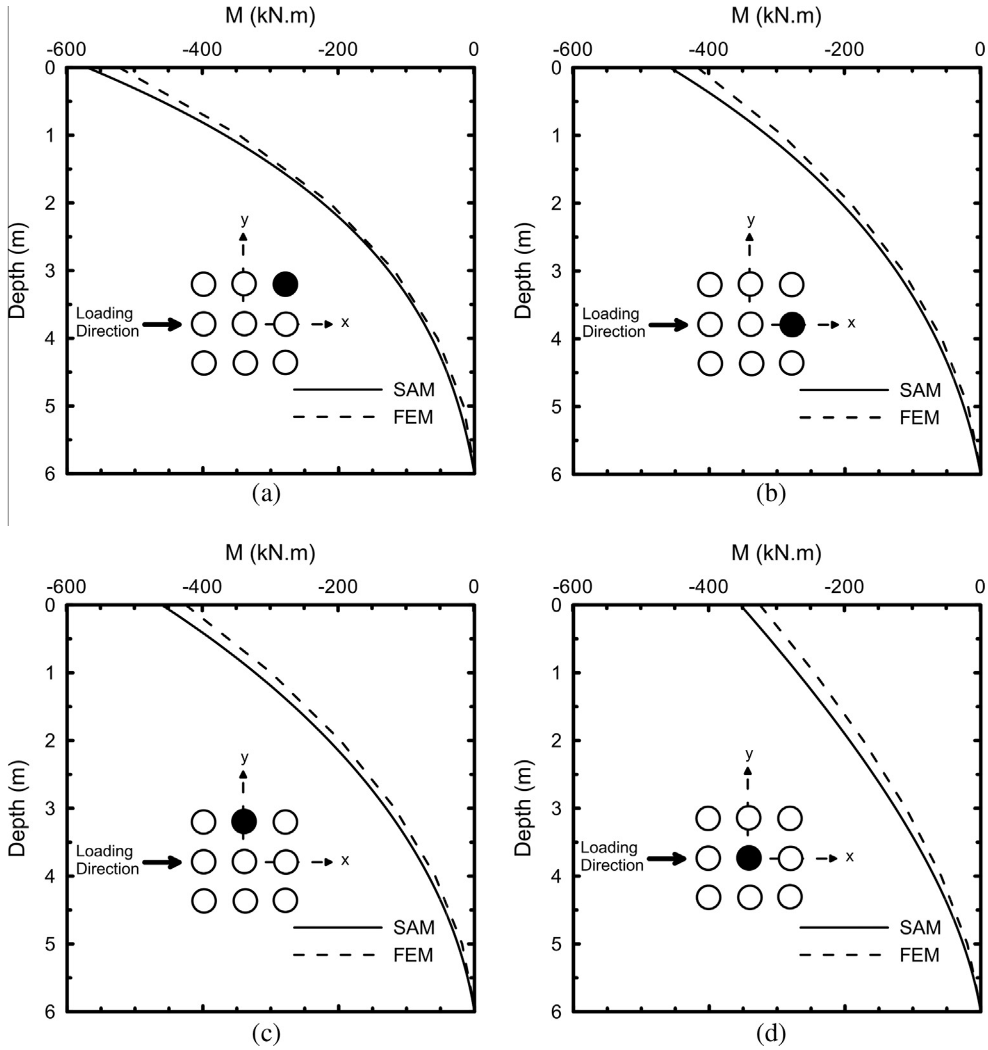

Fig. 18. Bending moment along the (a) corner pile, (b) edge pile on the x axis, (c) edge pile on the y axis and (d) center pile in the 3 × 3 pile group.

multiple zones, each discretized with grids of different sizes, as shown in Fig. 3.

A five-point stencil is used for the finite difference scheme (Appendix A). To enhance the accuracy of the results and minimize the effect of pile shape discretization on the decay function and its partial derivatives at the pile–soil interface, nodes (such as node 1′ in Fig. 4, which illustrates this process for a circular pile and nodes 0 through 4) are added to the pile–soil interface. The value of the decay function within the pile domain is equal to unity, and that applies also to node 1′ in Fig. 4 (and all other nodes like it).

A grid size analysis was done to establish the largest grid size producing acceptable accuracy. A grid with size starting with B_p/100 immediately next to the pile and increasing gradually to $2B_p$ at a distance of $18B_p$ from the pile at the edge of a pile group was found to be acceptable for all configurations considered.

3.2. FEM validation

In order to illustrate the versatility and potential of the method, we analyzed four pile foundation configurations (a single pile, a 1 × 2 group, a 1 × 3 group, and a 3 × 3 group) installed in a layered soil profile. The soil profile consists of three layers (see Fig. 5). The elastic properties of the soil layers are: E_{s1} = 10 MPa and ν_{s1} = 0.35 for layer 1, E_{s2} = 30 MPa and ν_{s2} = 0.25 for layer 2, and E_{s3} = 60 MPa and ν_{s3} = 0.15 for layer 3. The first and second layers are 3-m thick, and the third layer extends below the level of the bases of the piles. The piles are all circular with B_p = 0.5 m, L_p = 15 m and E_p = 25 GPa. This combination of piles and soil profile lead to conditions referred to in the literature as "long" pile conditions, meaning that displacements, rotation and internal forces approach zero for a depth less than the pile length. The spacing s is $3B_p$. The pile heads are all fixed to simulate a rigid pile cap. A lateral displacement of 10 mm was applied, together with rotation constraint (Eq. (20)), to the head of each pile (implicitly simulating pile cap rigidity). The soil domain is 60 m (=$120B_p$) long, 60 m (=$120B_p$) wide, and 30 m deep.

Results of the analyses of piles installed in the 3-layered soil profile shown in Fig. 5 are presented in Fig. 6 (for a single pile), Fig. 7 (for a 1 × 2 pile group), Figs. 8–11 (for a 1 × 3 pile group) and Figs. 12–15 (for a 3 × 3 pile group). The figures show the profile of soil displacements at ground surface level in the direction of application of the load and the displacement, bending moment and shear force along the axis of each pile obtained both from the analyses and from the finite element method. There is good agreement between the results from the analyses and those from the finite element method. The sharp discontinuities in the shear force plots for the piles at the location of layer interfaces results from the transition from a layer with larger shear modulus to one with lower shear modulus: there is a difference in shear force carrying capacity between one layer and the next that must be absorbed by the

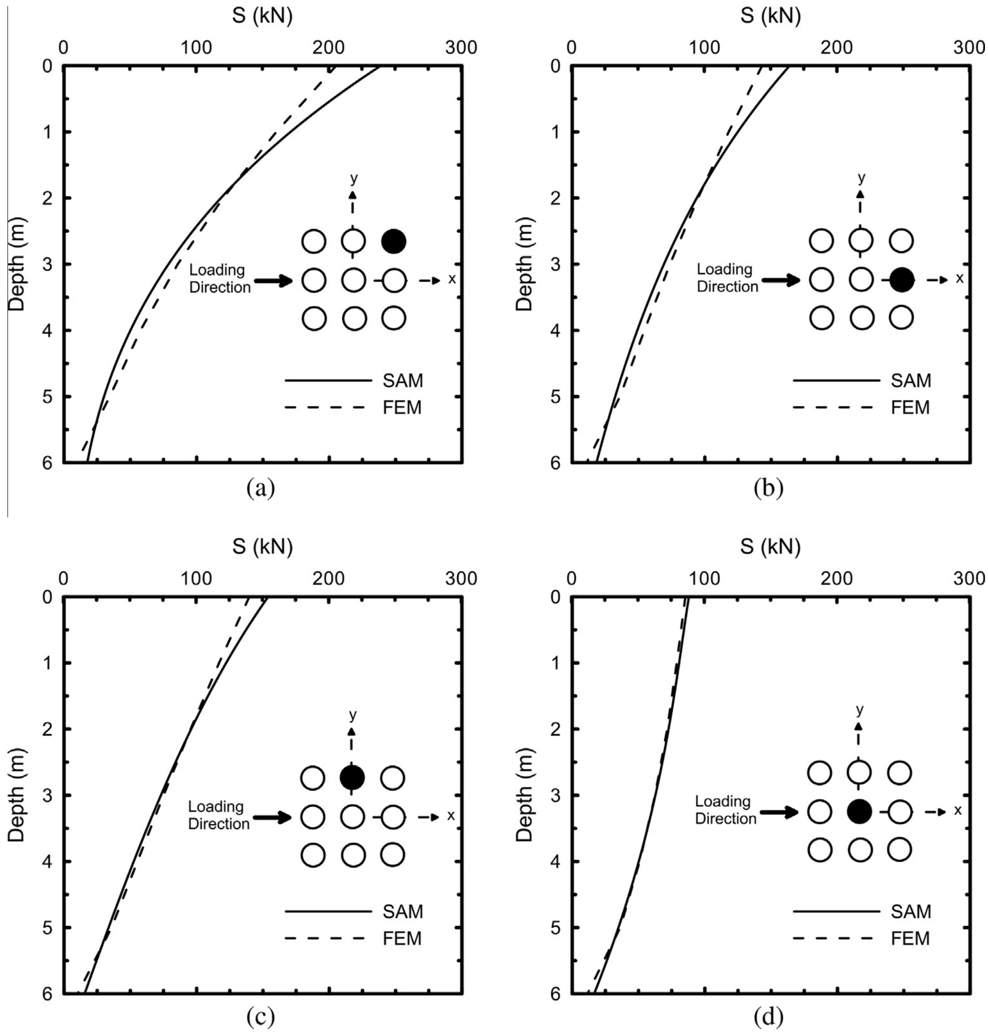

Fig. 19. Shear force along the (a) corner pile, (b) edge pile on the x axis, (c) edge pile on the y axis and (d) center pile in the 3×3 pile group.

pile(s). These discontinuities are not observed in the FEM because it relies on variable interpolations that produce a smooth plot.

For each calculation case, we perform calculations also using a finite element analysis. The finite element analyses were performed using ABAQUS CAE on a 24-core x86 server containing twelve 3.0-GHz dual-core Xeon 5675 processors with 48-GB RAM. The analyses relied on 20-noded brick elements, with domains identical to those of the analyses. Plots of displacement in the soil domain and along the pile axis are provided for each case to illustrate the close match between the results of the analyses and the FEM. The analyses were performed with a Visual C# code running on a desktop computer with 2 Intel Quad 2.66-GHz processors and 4-GB RAM. A summary of the computational effort in each single pile and pile group analysis using FEM and SAM is presented in Table 1.

The analysis works equally well for "short" piles, that is, piles for which displacements, rotations and internal forces do not go to zero anywhere along the pile. This is illustrated for a 3×3 pile group consisting of short piles embedded in a uniform soil profile with $E_s = 10$ MPa and $\nu_s = 0.2$. The piles are all circular with $B_p = 1$ m and $L_p = 6$ m and $E_p = 25$ GPa. The spacing s is $2B_p$. The pile heads are all fixed to simulate a rigid pile cap. A lateral displacement of 10 mm was applied, together with rotation constraint to the head of each pile. The soil domain is 120 m (=$120B_p$) long, 120 m (=$120B_p$) wide, and 40 m deep. Results of the analyses are presented in Figs. 16–19. The figures show the profile of soil displacements at ground surface level in the direction of application of the load, and the displacement, bending moment and shear force along the axis of each pile obtained both from the analyses and from the finite element method. The results show that there is good agreement between the analyses and the finite element method in predicting the pile and soil response.

Fig. 20 shows a comparison between the predictions of the load carried by piles at four different locations of a 4×4 pile group predicted by the current method, FEM using ABAQUS and an isotropic linear elastic constitutive model for the soil, and the methods of [52–54]. The pile–soil relative stiffness $K_R = E_pI_p/E_sL^4 = 10^{-5}$, the soil Poisson's ratio $\nu_s = 0.5$ (0.49 for SAM and FEM), and the pile length-to-diameter ratio $L_p/B_p = 25$. The load carried by each pile is divided by the average load applied to the pile group. Fig. 20 shows that the load carried by individual piles within the group predicted by all the methods are in generally good agreement for larger spacings, with the present method comparing favorably with the FEM predictions at closer spacings; the method of, [53] fares better than the other three methods but the differences are relatively small.

4. Group efficiency

A particularly useful result from calculations using the analyses proposed in this paper is the possibility of preparing pile group

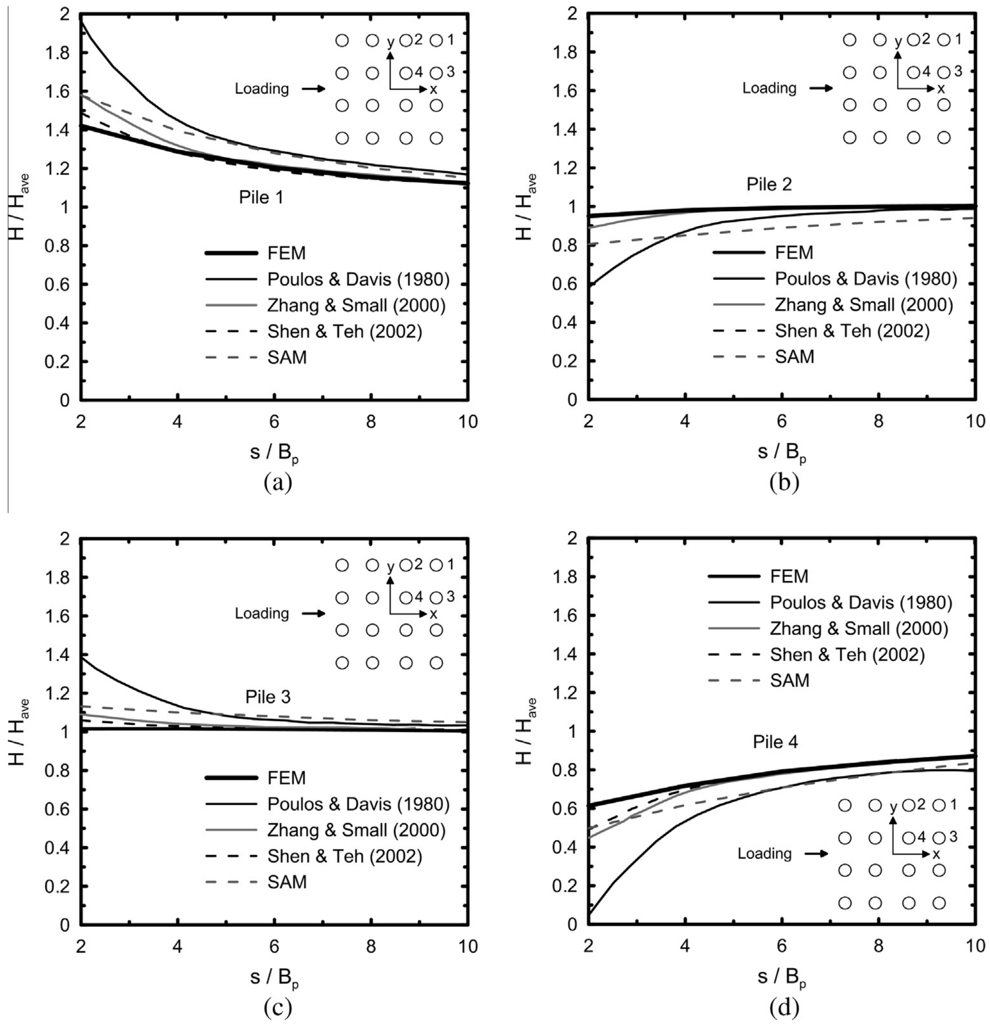

Fig. 20. Distribution of horizontal load in a 4 × 4 pile group: (a) pile 1, (b) pile 2, (c) pile 3 and (d) pile 4.

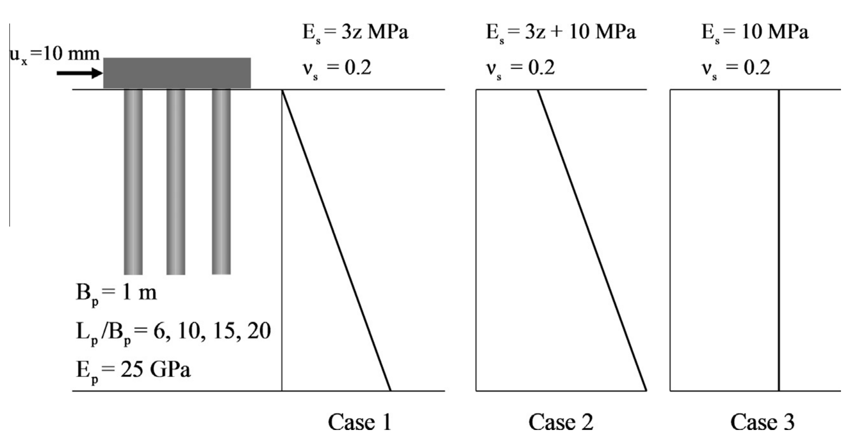

Fig. 21. Soil profiles for the 3 × 3 pile group.

efficiency charts, which give engineers a basis for design of laterally loaded pile groups if information on the response of an isolated pile is available. The pile group efficiency factor η_l here is defined simply as the ratio of the average lateral load capacity of a pile in the group to the lateral load capacity of a single pile under the same conditions. Mathematically:

$$\eta_l = \frac{H_{\text{total}}/n_p}{H_{\text{single}}} \tag{56}$$

where H_{total} is the lateral capacity of the pile group, and H_{single} is the lateral capacity of a single pile at the same displacement level and identical conditions.

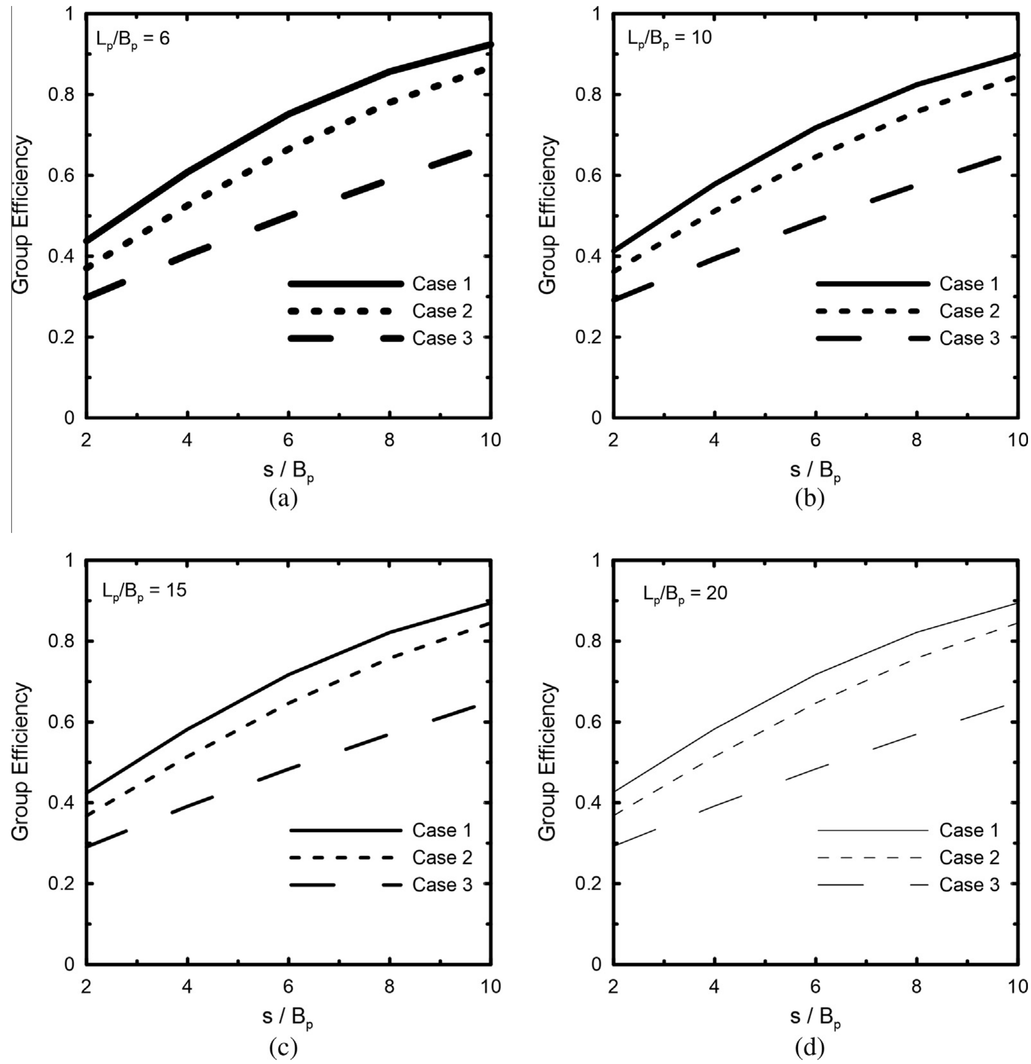

Fig. 22. Effect of pile-to-pile spacing on group efficiency of the 3 × 3 pile group with (a) $L_p/B_p = 6$, (b) $L_p/B_p = 10$, (c) $L_p/B_p = 15$, and (d) $L_p/B_p = 20$.

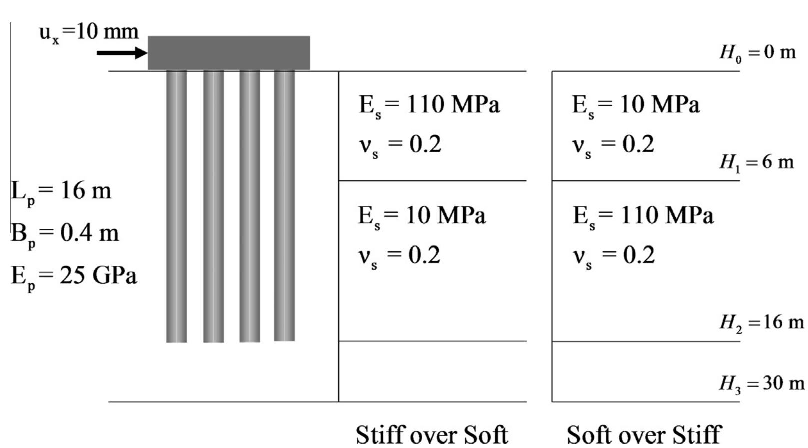

Fig. 23. Soil profiles for the 4 × 4 pile group.

Fig. 21 shows a 3 × 3 pile group with a rigid cap embedded in soil profiles with different stiffness that is loaded laterally to a displacement u_x = 10 mm. The piles are all circular with B_p = 1 m and E_p = 25 GPa. Three general stiffness profiles are considered. In case 1, soil stiffness is zero at the ground surface and increases linearly with depth. In case 2, the soil stiffness at the ground surface is non-zero (taken as 10 MPa) and increases linearly with depth. In case 3, soil stiffness is uniform with depth. In cases 1 and 2, the soil profile, which is 40-m deep, was sub-divided into relatively thin sub-layers with thickness of 1 m, and the elastic soil properties in the middle of every sub-layer were used to solve the differential equations for the piles.

Fig. 22(a)–(d) shows group efficiency as a function of pile spacing for the three stiffness profile cases considered in this paper for piles with L_p/B_p of 6, 10, 15, and 20 and pile spacing ranging from $2B_p$ to $10B_p$. The critical length separating "long" from "short" pile response is approximately 10 m for these conditions. As expected, Fig. 22 shows that group efficiency increases with increasing spacing. Fig. 22(a)–(d) shows that efficiency initially drops slightly as length approaches the critical length, then increases very slightly and stays unchanged for lengths clearly greater than the critical length. Additionally, as shown in Fig. 22(a)–(d), when the soil stiffness decreases, group efficiency increases, particularly for greater spacings.

The analysis, applied to a 4×4 pile group in two-layered soil profiles, allows insights into pile group response in cases in which a softer soil layer (such as soft clay or very loose sand) overlies a stiffer soil layer (such as very stiff clay or dense sand) and vice versa (see Fig. 23). The piles considered in the calculations have E_p = 25 GPa, L_p = 16 m and B_p = 0.4 m, with L_p/B_p = 40. The soft layer has $E_{s,soft}$ = 10 MPa and $\nu_{s,soft}$ = 0.2, while the stiffer layer has $E_{s,stiff}$ = 110 MPa and $\nu_{s,stiff}$ = 0.2. The thickness of the upper layer is 6 m. A horizontal displacement of 10 mm was applied to the pile cap. The group efficiency was calculated for spacings equal to $2B_p$, $4B_p$, $6B_p$, $8B_p$ and $10B_p$. Fig. 24 shows that the group efficiency is greater for the soft-over-stiff layer soil profile than for the stiff-over-soft layer soil profile. It also shows that the group efficiency of the pile group is the same for the two soil profiles for a pile spacing of $2B_p$, but the values of the efficiency diverge as the pile spacing increases. Due to the large value of L_p/B_p, the maximum group efficiency is well below unity, which is consistent with what is observed also in Fig. 22.

5. Summary and conclusions

This paper presented a method for the analysis of single piles and pile groups subjected to lateral loads. The method is based on a formulation of the displacement field that ties the displacement within a soil mass to the displacements of the pile(s) and relies on application of the principle of virtual work and calculus of variations to this displacement field formulation. One of the key advantages of this method is that it allows use of any constitutive model, being based on the principle of virtual work and not relying on the superposition principle or any elasticity-bound concept, so the analysis can be extended to simple nonlinear elastic models or even to full-blown, realistic constitutive models.

The method produces results that compare well with finite element predictions. The effort involved in preparing and performing an analysis is minimal compared to that required for finite element analysis. The usefulness of the method was illustrated by preparing efficiency plots for pile groups considering typical soil modulus profiles. These plots can be used, given the lateral load capacity of a single pile (which may be obtained from a pile load test), to produce an estimate of the total capacity of the group.

Conflict of interest

There is no conflict of interest.

Acknowledgment

This material is based upon work supported by the National Science Foundation under Grant No. 0969949. The authors are very grateful for this support.

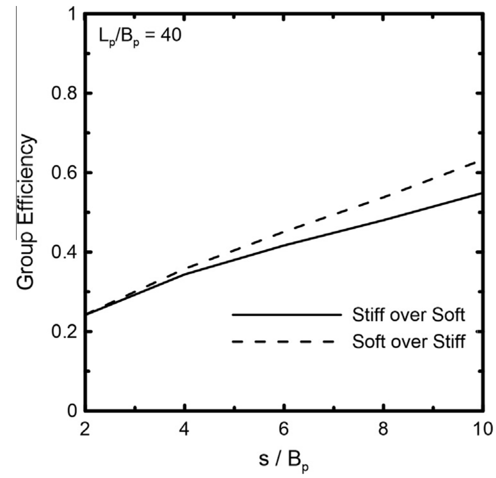

Fig. 24. Effect of pile-to-pile spacing on the group efficiency of the 4×4 pile group (L_p = 16 m and B_p = 0.4 m, with L_p/B_p = 40).

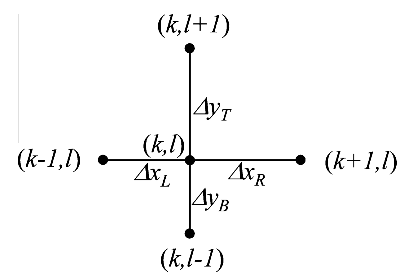

Fig. A.1. Unequal-armed five-point stencil for finite difference discretization.

Appendix A

The unequal-arm, five-point stencil used to derive the finite difference discretizations used in the present paper is shown in Fig. A.1.

The forward and backward Taylor series expansions of $f_i(x,y)$ about x are:

$$f_i^{k+1,l} = f_i^{k,l} + \frac{\Delta x_R}{1!}\frac{\partial f_i^{k,l}}{\partial x} + \frac{\Delta x_R^2}{2!}\frac{\partial^2 f_i^{k,l}}{\partial x^2} + \cdots \tag{A.1}$$

and

$$f_i^{k-1,l} = f_i^{k,l} - \frac{\Delta x_L}{1!}\frac{\partial f_i^{k,l}}{\partial x} + \frac{\Delta x_L^2}{2!}\frac{\partial^2 f_i^{k,l}}{\partial x^2} + \cdots \tag{A.2}$$

The forward and backward Taylor series expansions of $f_i(x,y)$ about y are:

$$f_i^{k,l+1} = f_i^{k,l} + \frac{\Delta y_T}{1!}\frac{\partial f_i^{k,l}}{\partial y} + \frac{\Delta y_T^2}{2!}\frac{\partial^2 f_i^{k,l}}{\partial y^2} + \cdots \tag{A.3}$$

and

$$f_i^{k,l-1} = f_i^{k,l} - \frac{\Delta y_B}{1!}\frac{\partial f_i^{k,l}}{\partial y} + \frac{\Delta y_B^2}{2!}\frac{\partial^2 f_i^{k,l}}{\partial y^2} + \cdots \tag{A.4}$$

Neglecting terms of order higher than one in Eqs. (A.1)–(A.4), we can write first-order, central-difference approximations to the partial derivatives of $f_i(x,y)$ for unequal spacing:

$$\frac{\partial f_i^{k,l}}{\partial x} = \frac{f_i^{k+1,l} - f_i^{k-1,l}}{\Delta x_L + \Delta x_R} + O(\Delta x) \tag{A.5}$$

$$\frac{\partial f_i^{k,l}}{\partial y} = \frac{f_i^{k,l+1} - f_i^{k,l-1}}{\Delta y_B + \Delta y_T} + O(\Delta y) \tag{A.6}$$

Using the central-difference formulation, the second-order partial derivatives of function $f_i(x, y)$ can be approximated as follows:

$$\frac{\partial^2 f_i^{k,l}}{\partial x^2} = 2\left[\frac{f_i^{k-1,l} - 2f_i^{k,l} + f_i^{k+1,l} - \frac{\Delta x_R - \Delta x_L}{\Delta x_R + \Delta x_L}\left(f_i^{k+1,l} - f_i^{k-1,l}\right)}{\Delta x_L^2 + \Delta x_R^2}\right] + O(\Delta x^2) \quad (A.7)$$

$$\frac{\partial^2 f_i^{k,l}}{\partial y^2} = 2\left[\frac{f_i^{k,l-1} - 2f_i^{k,l} + f_i^{k,l+1} - \frac{\Delta y_T - \Delta y_B}{\Delta y_T + \Delta y_B}\left(f_i^{k,l+1} - f_i^{k,l-1}\right)}{\Delta y_B^2 + \Delta y_T^2}\right] + O(\Delta y^2) \quad (A.8)$$

Simplifying these expressions:

$$\frac{\partial^2 f_i^{k,l}}{\partial x^2} \approx 4\left[\frac{\Delta x_R f_i^{k-1,l} - (\Delta x_L + \Delta x_R) f_i^{k,l} + \Delta x_L f_i^{k+1,l}}{(\Delta x_L + \Delta x_R)(\Delta x_L^2 + \Delta x_R^2)}\right] \quad (A.9)$$

$$\frac{\partial^2 f_i^{k,l}}{\partial y^2} \approx 4\left[\frac{\Delta y_T f_i^{k,l-1} - (\Delta y_B + \Delta y_T) f_i^{k,l} + \Delta y_B f_i^{k,l+1}}{(\Delta y_B + \Delta y_T)(\Delta y_B^2 + \Delta y_T^2)}\right] \quad (A.10)$$

References

[1] Winkler E. Die lehre von der elasticitaet und festigkeit. Prag, Dominicus; 1867.
[2] Matlock H, Reese LC. Generalized solutions for laterally loaded piles. J Soil Mech Found Div 1960;86:63–91.
[3] McClelland B, Focht Jr JA. Soil modulus for laterally loaded piles. Transactions 1958;123:1049–63.
[4] Reese LC, Cox WR. Soil behavior from analysis of tests of uninstrumented piles under lateral loading. Perform Deep Found ASTM STP 1969;444:160–76.
[5] Reese LC, Cox WR, Koop FD. Analysis of laterally loaded piles in sand. In: 6th Offshore technical conference. Houston, Texas; 1974, p. 473–83.
[6] Reese LC, Cox WR, Koop FD. Field testing and analysis of laterally loaded piles in stiff clay. In: 7th Offshore technical conference; 1975. p. 671–90.
[7] Reese JC, Van Impe WF. Single piles and pile groups under lateral loadings. Balkema: Rotterdam; 2001.
[8] Matlock H. Correlations for design of laterally loaded piles in soft clay. In: 2nd Offshore technical conference. Houston, Texas; 1970. p. 577–94.
[9] Selvadurai APS. Elastic analysis of soil-foundation interaction. Elsevier; 1979.
[10] Georgiadis M, Butterfield R. Laterally loaded pile behavior. J Geotech Eng Div 1982;108:155–65.
[11] Rao NSVK. Vibration analysis and foundation dynamics. New Delhi: Wheeler Publishing; 1998.
[12] Hetényi M. Beams on elastic foundation. Ann Arbor: Univ. Michigan Press; 1946.
[13] Poulos HG. Behavior of laterally loaded piles: i-single piles. J Soil Mech Found Div 1971;97:711–31.
[14] Budhu M, Davies TG. Analysis of laterally loaded piles in soft clays. J Geotech Eng 1988;114:21–39.
[15] Rao NSVK, Prasad SK. Semi-analytical finite element analysis of laterally loaded piles. In: 6th International conference on numerical methods on geomechanical. Innsbruck, Austria; 1988. p. 1431–6.
[16] Rao SN, Ramakrishna VGST, Rao MB. Influence of rigidity on laterally loaded pile groups in marine clay. J Geotech Geoenviron Eng 1998;124:542–9.
[17] Poulos HG. Behavior of laterally loaded piles: ii – pile groups. J Soil Mech Found Div 1971;97:733–57.
[18] Poulos HG, Randolph MF. Pile group analysis: a study of two methods. J Geotech Eng 1983:109.
[19] Sun K. Static analysis of laterally loaded piles. In: 11th Southeast Asian geotechnical conference. Singapore; 1993. p. 589–94.
[20] Sun K. A numerical method for laterally loaded piles. Comput Geotech 1994;16:263–89.
[21] Basu D, Salgado R. Elastic analysis of laterally loaded pile in multi-layered soil. Geomech Geoeng 2007;2:183–96.
[22] Basu D, Salgado R. Analysis of laterally loaded piles with rectangular cross sections embedded in layered soil. Int J Numer Anal Meth Geomech 2008;32:721–44.
[23] Basu D, Salgado R, Prezzi M. A continuum-based model for analysis of laterally loaded piles in layered soils. Géotechnique 2009;59:127–40.
[24] Desai CS, Appel GC. 3-D analysis of laterally loaded structures. In: 2nd International conference on numerical methods on geomechanics. Blacksburg, Virginia; 1976. p. 405–18.
[25] Brown DA, Morrison C, Reese LC. Lateral load behavior of pile group in sand. J Geotech Eng 1988;114:1261–76.
[26] Bhowmik SK, Long JH. An analytical investigation of the behavior of laterally loaded piles. Geotech Eng Congr 1991:1307–18.
[27] Trochanis AM, Bielak J, Christiano P. Three-dimensional nonlinear study of piles. J Geotech Eng 1991;117:429–47.
[28] Bransby MF. Selection of *p–y* curves for the design of single laterally loaded piles. Int J Numer Anal Meth Geomech 1999;23:1909–26.
[29] Hsiung YM, Chen YL. Simplified method for analyzing laterally loaded single piles in clays. J Geotech Geoenviron Eng 1997;123:1018–29.
[30] Feagin LB. Lateral pile-loading tests. Transactions 1937;102:236–54.
[31] Feagin LB. Lateral load tests on groups of battered and vertical piles. ASTM Spec Tech Publ; 1954. pp. 12–28.
[32] Kim JB, Brungraber RJ. Full-scale lateral load tests of pile groups. J Geotech Eng Div 1976;102:87–105.
[33] Cox WR, Dixon DA, Murphy BS. Lateral-load tests on 25.4-mm (1-in.) diameter piles in very soft clay in side-by-side and in-line groups. Later Load Deep Found Anal Perform, ASTM STP 1984;835:122–39.
[34] McVay MC, Shang TI, Casper R. Centrifuge testing of fixed-head laterally loaded battered and plumb pile groups in sand. Geotech Test J 1996;19:41–50.
[35] Gandhi SR, Selvam S. Group effect on driven piles under lateral load. J Geotech Geoenviron Eng 1997;123:702–9.
[36] Rollins KM, Peterson KT, Weaver TJ. Lateral load behavior of full-scale pile group in clay. J Geotech Geoenviron Eng 1998;124:468–78.
[37] Ng CWW, Yau TLY, Li JHM, Tang WH. Side resistance of large diameter bored piles socketed into decomposed rocks. J Geotech Geoenviron Eng 2001;127:642–57.
[38] Hrennikoff A. Analysis of pile foundations with batter piles. Transactions 1950;CXV:351–81.
[39] Francis A. Analysis of pile groups with flexural resistance. J Soil Mech Found Div 1964;90:1–32.
[40] Saul WE. Static and dynamic analysis of pile foundations. J Struct Div 1968;94:1077–100.
[41] Brown DA, Reese LC, O'Neill MW. Cyclic lateral loading of a large-scale pile group. J Geotech Eng 1987;113:1326–43.
[42] Brown DA, Shie CF. Modification of *p–y* curves to account for group effects on laterally loaded piles. Geotech Eng Congr 1991:479–90.
[43] McVay M, Zhang L, Molnit T, Lai P. Centrifuge testing of large laterally loaded pile groups in sands. J Geotech Geoenviron Eng 1998;124:1016–26.
[44] McVay M, Casper R, Shang TI. Lateral response of three-row groups in loose to dense sands at 3D and 5D pile spacing. J Geotech Eng 1995;121:436–41.
[45] Ruesta PF, Townsend FC. Evaluation of laterally loaded pile group at Roosevelt bridge. J Geotech Geoenviron Eng 1997;123:1153–61.
[46] Zhang L, McVay MC, Lai PW. Centrifuge modelling of laterally loaded single battered piles in sands. Can Geotech J 1999;36:1074–84.
[47] Ng CWW, Zhang LM. Three-dimensional analysis of performance of laterally loaded sleeved piles in sloping ground. J Geotech Geoenviron Eng 2001;127:499–509.
[48] Dunnuvant TW, O'Neill MW. Evaluation of design-oriented methods for analysis of vertical pile groups subjected to lateral load. In: 3rd International conference on numerical methods offshore piling. Paris, France; 1986. p. 303–16.
[49] Hariharan M, Kumarasamy K. Analysis of pile groups subjected to lateral loads. In: 3rd International conference on behaviour offshore structures. Massachusetts; 1983. p. 383–90.
[50] Horsnell MR, Aldridge TR, Erbrich CE. Lateral group behavior of piles in offshore soil conditions. In: 22nd Offshore technical conference. Houston, Texas; 1990. p. 417–24.
[51] Zhang L, McVay MC, Lai P. Numerical analysis of laterally loaded 3×3 to 7×3 pile groups in sands. J Geotech Geoenviron Eng 1999;125:936–46.
[52] Poulos HG, Davis EH. Pile foundation analysis and design. New York: John Wiley & Sons; 1980.
[53] Shen WY, Teh CI. Analysis of laterally loaded pile groups using a variational approach. Geotechnique 2002;52:201–8.
[54] Zhang H, Small J. Analysis of capped pile groups subjected to horizontal and vertical loads. Comput Geotech 2000;26:1–21.